

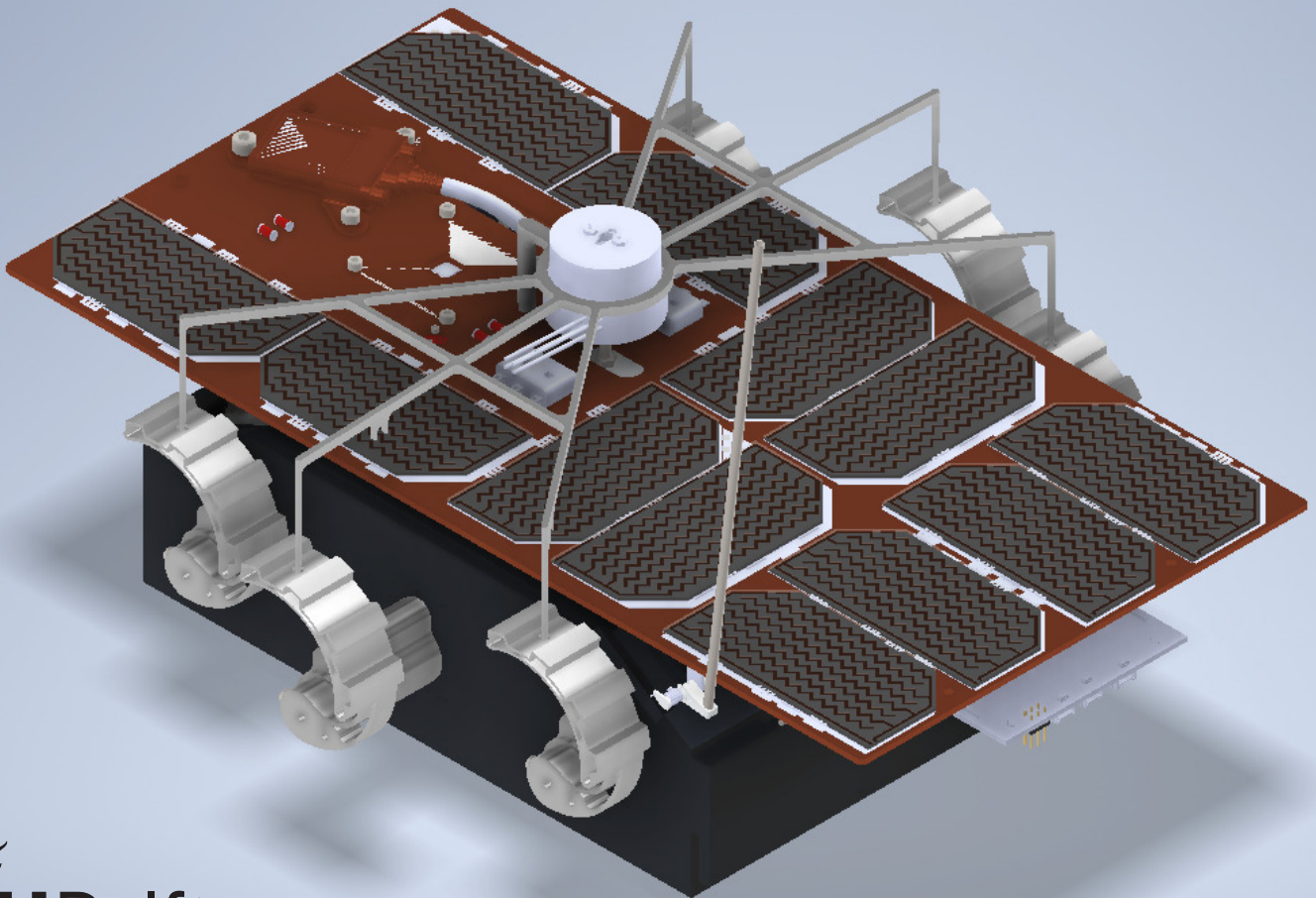
Electrodynamic Screen for Lunar Zebro Moon rover

Electrode Design Team

T.B. Plantfeber
M. Mihankhah
T.O. Geerling

A feasibility analysis:

An evaluation on the viability of utilizing EDS to improve the performance of the solar panels on the Lunar Zebro



Electrodynamic Screen for Lunar Zebro Moon rover

Electrode Design Team

by

T.B. Plantfeber

M. Mihankhah

T.O. Geerling

to obtain the degree of Bachelor of Science
at the Delft University of Technology,
defended on the 27th of June.

Student number:	T.O. Geerling	5034914
	M. Mihankhah	4913957
	T.B. Plantfeber	4590848
Project duration:	April 24, 2023 – June 30, 2023	
Thesis committee:	dr. ir. C.J.M. (Chris) Verhoeven,	TU Delft, supervisor
	Dr. M. Ghaffarian Niasar,	TU Delft
	Dr. R.A.C.M.M. van Swaaij,	TU Delft

An electronic version of this thesis is available at <http://repository.tudelft.nl/>.

Preface

This study would not have been possible without the support of the Lunar Zebro project. We would like to especially thank Ir. Dr. C.J.M. (Chris) Verhoeven, without him the Lunar Zebro might not have been. We would like to thank Verhoeven for all his support as our supervisor. We appreciated the freedom and autonomy we got regarding the topic.

We are very grateful for Dr. M. Ghaffarian Niasar's guidance and unique ideas. Floris van Mourik and his input, Dr. I.E. Lager's great remarks and arrangement, Simon Van Hulle's helpful systems engineering suggestions, and Dr. ir. Aditya Shekhar's remarks. We hope that this study will contribute to the success of Lunar Zebro and its ambitious goals.

T.B. Plantfeber
M. Mihankhah
T.O. Geerling

Delft, June 2023

Abstract

One of the major challenges faced by future robotic and human missions to Mars and the Moon is the presence of atmospheric dust. The Lunar Zebro rover which is intended to walk on the Moon is powered by solar panel. Due to its surrounding terrain, which mostly consists of small particles, the rover may be a potential target for dust accumulation, which reduces its output power. For the longevity of any space mission, it is important to have a long-lasting source of energy. That is why during this project, an Electro dynamic screen is constructed which could remove dust from a 100 x 100 mm area without containing moving parts. One subgroup concentrated on building the electronics necessary to create a high voltage (1.6kV) three-phase drive signal, the other group focused on the electrodes of the system and described the effects of an electric field on dielectric particles. These are mostly found on the Moon. Different electrode architectures are proposed, but the zigzag architecture was found to be the best suited for a possible dust removal system. Furthermore, the higher voltage applied to the electrodes, the greater the forces exerted on the particles are. Further research should be conducted for any possible implementation. It is recommended to also read the other theses.

Contents

List of Symbols & Acronyms	ix
1 Introduction	1
1.1 Lunar Dust and challenges for exploration missions	1
2 Program of requirement	3
2.1 Mandatory requirements	3
2.2 TRL levels	4
2.3 Trade-off analysis.	4
2.4 Objectives.	4
2.5 Assumptions	4
3 Background	5
3.1 The solar cells of the Lunar Zebro rover.	5
3.2 Dust Particles	6
3.2.1 Particle deposition on rover	7
3.3 Effect of lunar dust on the efficiency of solar panels	8
3.3.1 Theoretical Analysis	8
3.3.2 Experimental Analysis	8
3.4 Electric field and Breakdown.	9
3.4.1 Field electron emission.	9
3.4.2 Dielectric barrier discharge.	10
3.4.3 Field Enhancement.	10
3.5 Dust particle model	10
3.5.1 Gravity	10
3.5.2 Air drag	11
3.5.3 Particle electrostatic forces	11
3.5.4 Adhesion and Cohesion in Electrostatic Lofting.	12
3.5.5 Dielectrophoresis	12
3.5.6 Tribocharging	12
3.6 Friction and static clinging	13
3.7 Conclusion and model of dust particles	13
4 State of the Art	14
4.1 Design parameters	14
4.2 Removal Mechanism.	15
4.3 Testing and Simulation	15
5 Electrodynamic Screen model	16
5.1 Electrode Architecture	16
5.1.1 Orientation of Electrodes.	17
5.2 Design parameters	17
5.3 Transmission model	18
5.4 Breakdown	19
5.5 Equivalent capacitance.	19
5.6 Simplification of Electric field.	19
5.6.1 Comparing and fitting to COMSOL	20
5.7 DEP forces	21
5.8 Particle force model	22
5.8.1 Particle repulsion	22
5.8.2 Neglecting gravity on Field strength	23
5.8.3 Determining Electric field required for dust removal on the moon	23

5.9	Modeling switching frequency	24
5.9.1	Determining Switching frequency	25
6	Experimental Evaluation	26
6.1	Experimental setup	27
6.2	Iteration 1 - Proof of concept	27
6.2.1	Design	27
6.2.2	Test procedure	27
6.2.3	Results	28
6.3	Iteration 2 - Zigzag parameter variation	29
6.3.1	Design	30
6.3.2	Visual findings	30
7	Integration and efficiency	32
7.1	Transparent ITO	32
7.2	Solar panel efficiency	33
7.3	Dust deposition on panel	33
8	Feasibility and the proposed design	35
8.1	Proposed Design	35
8.1.1	Setting the parameters	35
8.1.2	Modes of operation	36
8.2	Recommendations regarding testing	36
9	Conclusion	37
9.1	Discussion	37
9.2	Future research	38
A	Appendix A	43
A.1	Mass of a particle	43
A.2	Hamaker constant	43
A.3	Surface Cleanliness	43
A.4	Experimental Efficiency results from papers	44
A.5	Electrostatics	45
A.5.1	Capacitance	45
A.6	Transmission line	45
A.6.1	Electrode Resistance	46
A.6.2	Series resistance	46
A.6.3	Co planar Capacitance	46
A.7	Optics	47
A.7.1	transmittance	47
A.7.2	Complex refraction index	47
A.7.3	Attenuation	48
A.8	Solar panel	49
A.8.1	Short circuit current	49
A.8.2	J-V Curve	49
A.8.3	Open circuit voltage	49
A.8.4	Solar panel Efficiency	49
A.8.5	Conductance of insulation medium	50
A.9	Effects of transmission line	50
A.9.1	Characteristic impedance of the line	50
A.9.2	Reflection	50
A.9.3	Phase shift	50
A.10	Electric field strength needed at different solar panel angles	50
A.11	Code	51

B Implementing Electrodes	58
B.1 Prototype	58
B.1.1 Creating a spiral electrode	58
B.1.2 Images of design iteration 1	60
B.2 Kicad automation scripts	61
C Appendix C	70
C.1 Step-by-step plan testing iteration 1	70
C.2 Results Iteration 1	70
C.3 Results Iteration 2	71
C.4 Simulation Geometry Iteration 1	71
C.5 Indium tin oxide, ITO (In ₂ O ₃ -SnO ₂) dataset	71
C.6 Solar panel Quantum efficiency	71
C.7 Output Power Restoration (OPR) and Transmission Efficiency (TE).	72

List of Symbols & Acronyms

Symbol	Definition	Unit
Greek characters		
ρ_p	Density of dust	[kg m ²]
β	Field enhancement coefficient	[-]
ϵ	electrical permittivity	[F m ⁻¹]
τ_p	drag coefficient	[-]
γ_{se}	secondary electron emission coefficient	[-]
Latin characters		
A_p	Particle Area	[m ²]
E	Electric field	[V m ⁻¹]
f	switching frequency	[Hz]
I_0	Light incident on solar collector	[W]
I	Light intensity	[W]
V_b	Breakdown voltage	[V m ⁻¹]
p_g	Gas pressure	[Pa]
p	Pitch	[mm]
Q	Particle charge	[C]
Q_{ext}		[C]
w	width	[mm]
s	Spacing to ground	[mm]
g_s	Gravitation constant	[m s ⁻²]
F_c	Coulomb force	[N]
F_d	Drag force	[N]
F_{grav}	Gravitation force	[N]
F_{co}	Cohesion force	[N]
F_{DEP}	Dep force	[N]
K	Clausius-Mossotti function	[-]
m_p	Mass of particle	[kg]
r	radius of particle	[m]

Acronyms & Abbreviations

DBDs	Dielectric barrier discharges
DEP	Dielectrophoresis
FEM	Finite Element Method
PCB	Printed Circuit Board
EMI	Electromagnetic interference
XRF	method and non destructive analytical technique used to determine the elemental composition of any material

Introduction

1.1. Lunar Dust and challenges for exploration missions

One of the major challenges faced by future robotic and human missions to Mars and the Moon is the presence of atmospheric dust. Several missions have confirmed the existence of dust particles and their significant impact on the exploration missions [1]. The Lunar Zebro moon rover, which has a 14-day mission to study the lunar surface, is one of the space missions that might be affected by lunar dust. The accumulation of dust on various surfaces, such as photovoltaic cell surfaces, radiator surfaces, sealing surfaces, and mechanical and optical surfaces, can have a negative effect on different parts of the mission [2]. To address this issue, several solutions have been proposed for removing dust from surfaces. These include mechanical methods such as wiping, blowing, or regular cover removal. Another approach involves using an inexpensive, transparent covering for the solar panels, which can be removed after use. However, these methods often require additional mechanical components and/or a lubrication system.

An alternative solution is to employ electromechanical devices to shake or vibrate the solar panels. Ultrasound waves can also be utilized to overcome the adhesive forces and remove the dust layers. In some cases, the surfaces may need to be inverted during the process to effectively eliminate the dust layers. One of the options is the use of an electrodynamic principle. This technology, known as **electrodynamic screen (EDS)**, generates a **traveling wave** that acts as a contactless conveyor for moving particles. It is based on the concept of an **electric curtain**, which employs a series of parallel electrodes connected to an AC source. This concept was first proposed in 1972 [3], and has been researched by many other space missions.

The main question in the context of this project can be described as follows: **Is Lunar Dust a Problem for the Lunar Zebro Moon Rover's Mission? If so, how may these effects be minimized to prevent problems with energy harvesting?**

The lunar surface is covered by a thin layer of dust called Lunar regolith [4]. Due to the extremely low gravity on the Moon, these dust particles can remain suspended in the lunar atmosphere for extended periods and can be transported to various altitudes, including heights of up to 100 kilometers [4]. The movement of dust on the Moon is influenced by several factors, such as solar radiation, electrostatic forces, micrometeorite impacts, and thermal cycling. These factors can cause dust particles to become electrically charged and can create a phenomenon known as "**dust levitation**" or "**dust lofting**".

When dust particles become electrically charged, they can repel or attract each other based on their charge polarity. This electrostatic interaction can cause the dust particles to lift off the Lunar surface and remain suspended in the Lunar atmosphere for a considerable amount of time before eventually settling back down [5]. The suspended dust particles pose several challenges for Lunar missions and equipment, including solar panels. The accumulation of dust on solar panels can obstruct sunlight and reduce their efficiency over time. Therefore, it becomes important for long lunar missions to consider mitigation strategies to minimize the impact of dust deposition.

As lunar dust may pose a harm to the lunar operations, this report focuses on finding a solution to minimize the impact of lunar dust on the **solar panels of the Lunar Zebro Moon rover**. The EDS option has been chosen as the best choice after a trade-off study of several possibilities. The remaining

sections of this report will be dedicated to researching whether this solution can successfully achieve **Technology Readiness Level (TRL) 3** and advance the development of the technology for practical implementation. This is specifically for the **Lunar Zebro** application. The goal of this project is thus to determine if the EDS is feasible, which physical phenomena impact the dust removal rate, and what parameters impact the effectiveness of a design. The entire EDS system is made up of two parts: electrodes, which provide the right electrostatic field and thus remove the dust particles, and the electronics system, which generates the high voltage required by the electrodes. This report discusses the electrode design of the EDS system.

Research on lunar dust and its effects on solar panels will be presented in the following sections of this paper. Subsequently, EDS was selected as the dust mitigation method and its efficacy was proven by theoretical analysis, simulation, and practical testing. Finally, it has been determined whether this would be necessary in the case of a Lunar Zebro expedition of 14 days, and if so, what the feasible design would be.

2

Program of requirement

The main objective is to minimize the impact of lunar dust on the solar panels of the Lunar Zebro moon rover. This program guides the development of the dust mitigation system to protect the rover's solar panels efficiency.

2.1. Mandatory requirements

Table 2.1: Proposed requirements

Requirement	Compliance	Verification	Code
Functional	The system is able to increase the efficiency of a solar panel on a lunar rover by removing accumulating lunar dust particles	Inspection	R1
Functional	The system contains a rectangular area of 160 mm wide and 320 cm long on which dust can be removed	Inspection	R2
Functional	The system should be nonlethal when touched	Analysis	R3
Functional	The system contains no moving parts	Inspection	R4
Performance	The system is able to reduce the surface covered by a single layer of lunar regolith simulant particles with diameters ranging from 1 μm to 100 μm % s.	Test	R5
Performance	The maximum power usage of the system should be below 1W	Analysis, Test	R7
Performance	The spectrum between 100 MHz and 440 MHz should stay below TBD dB to avoid EMI	Analysis, Test	R7
Performance	The system itself shall not reduce the efficiency of the solar panel by more than 10%	Analysis	R9
Environmental	The system shall be able to meet all requirements between -40 °C and 80 °C	Analysis	R10
Cost factor	The finalised system shall not weigh more than 500 g	Analysis	R16
Cost factor	The finalised excluding the dust removal area cover shall not be larger than a rectangular box of TBD \times TBD \times TBD mm	Analysis	R17
Cost Factor	The system consumes no power when switched off	Analysis	R18

2.2. TRL levels

The Technology Readiness Level (TRL) is a scale that measures the maturity level of a particular technology. It is commonly used in the research and development (R&D) sector to assess the progress and readiness of a technology for practical applications. TRL ranges from 1 to 9, with 1 being the lowest level of maturity and 9 representing a fully developed and commercially available technology. The aim of this report is to possibly reach TRL levels 1 to 4 for a dust removal technology for lunar zebro:

TRL 1 to 4 represent the early stages of technology development, where the focus is on understanding the fundamental principles, formulating the concept, and conducting initial experimental and analytical validation. As the TRL level increases, the technology progresses towards higher levels of maturity and readiness for further development and eventual deployment.

2.3. Trade-off analysis

The trade-off analysis (Table 2.2), considering the requirements, yields clear results. Additionally, after reviewing the literature and observing the successful implementation of the EDS system in numerous space applications, the team has chosen to focus their efforts on evaluating the feasibility of integrating the EDS system into the Zebro rover, based on these requirements.

Table 2.2: Trade-off Analysis of Dust Removal Options for Solar Panels

Option	Dust Removal Efficiency	Power Consumption	Reliability	Show Stopper
Mechanical Wiping	High	Low	Moderate	Yes (conflict with no moving parts requirement)
Blowing Air Jets	Moderate	Moderate	High	Yes
Routine Cover Removal	Low	Low	High	Yes
Electrodynamic Screen (EDS)	Very High	Moderate	Very High	No

2.4. Objectives

The following requirements are to be met to the greatest extent possible. These requirements serve as the basis for the final trade-off analysis.

1. **Efficiency of dust removing should be as high as possible.** With the following formula is concerned.

$$\text{Removal rate (\%)} = \frac{\text{weight of the removed dust (mg)}}{\text{weight of the initial deposited dust (mg)}} \times 100 \quad (2.1)$$

2. **The method should have a minimal impact on the efficiency of the solar panels.** Efficiency, in this context, refers to achieving the highest rate of conversion from available solar energy to electrical energy over a specific period of time (X).
3. **The operation mode of the chosen design exhibits the highest overall energy gain,** which is attributed to the positive trends in reducing energy loss caused by shading and the cleaning cycle, as well as increasing energy gain from dust removal.

2.5. Assumptions

- The mission duration has been regarded as a variable parameter, allowing flexibility in conducting trade-offs based on specific mission durations that are yet to be determined. This approach enables adaptability in considering and evaluating different options for each unique mission duration.
- The accumulation of dust on the solar panels has been considered a significant factor. However, investigating the specific amount of dust gathered on the solar panels over a given period of time proved to be inconsequential for the purpose of this report. Hence, a parameter has been established to represent the degree of dust coverage on a solar panel, ranging from 0 to 100 percent.

3

Background

3.1. The solar cells of the Lunar Zebro rover

The **Lunar Zebro rover**[6], shown in Figure 3.1. The rover uses solar energy as its main source of energy. Due to its small size, it may be prone to dust accumulation.

The Lunar Zebro rover has a triple-junction InGaP / GaAs / Ge solar cell mounted on top of its assembly. This panel is model 3G30A from AzurSpace [8]. A visual representation can be seen in Figures 3.2. The dimension of the solar cell is 4x8 cm with an area of 30.18cm^2 . The Rover has an equivalent total solar cell area of 365cm^2 . This area should be kept clean of dust. A typical stack of an InGaP / GaAs / Ge is shown in Figure C.5. Such a stack up has a typical quantum efficiency (EQE) shown in Figure 3.3. The actual quantum efficiency and stack up with its internal layers are not known.



Figure 3.1: Solar panel assembly side view. Adapted from [7]

When speaking of Lunar Zebro's solar panels, Characterizing the radiance is of utmost importance. The main source of radiation in the lunar atmosphere is that of the sun. Mainly, two types of radiation occur, ionizing and non-ionizing, which depend on the energy a particle possesses[10]. Due to the absence of an atmosphere, the radiation profile is different from that of Earth. The sun radiates to the Moon, and the spectrum of this light is approximately quantified with the AM0 model [9]. The solar radiance being referred to is the one present outside the Earth's atmosphere. It possesses an average power of 1361 watts per square meter. The spectrum of sunlight is given by AM0 seen in Figure 3.4.

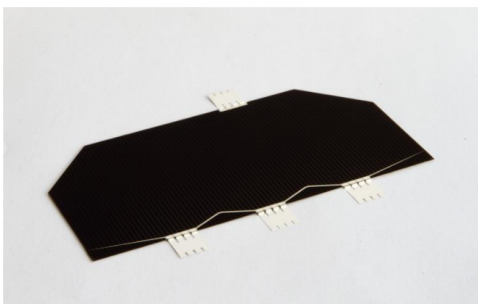


Figure 3.2: Solar cell photo taken from [8]

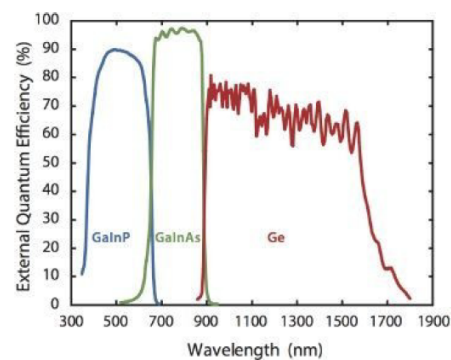


Figure 3.3: Typical EQE of a triple junction solar cell [9]

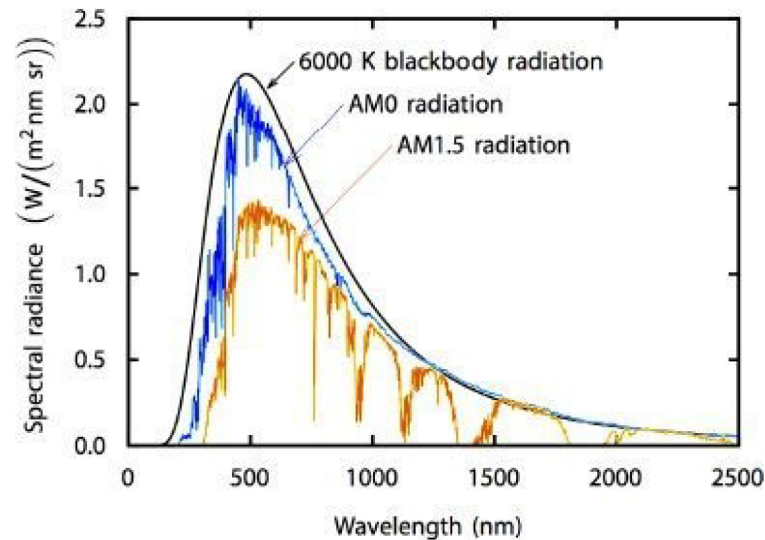


Figure 3.4: Solar spectrum of interest AM0 [9]

To facilitate future analysis, it is useful to identify the range of wavelengths depicted in Figure 3.4. The minimum and maximum wavelengths can be defined as ranging from 250 nm to 2250 nm.

There are clear transitions at **600 nm** and **900 nm** in Figure 3.3. This will be taken as the boundary's of the transition between solar cell junctions. When shading occurs and one of the junctions in a triple-junction solar cell generates fewer electron-hole pairs, it leads to current limitations in the other junctions. This reduction in current affects the overall energy yield of the solar panel, causing it to decrease. In a triple junction solar cell, The main current-limiting junction inside a triple junction solar cell is the top junction. Because measuring the quantum efficiency of solar panels is not part of the project's purpose, a simple estimation is utilized to account for the drop in efficiency. The Table C.4 offers an approximation of quantum efficiency.

3.2. Dust Particles

The **lunar 'regolith'** is a **3-20 m** thick layer of soil and rocks. Its components range from small dust to massive "blocks". 70% of the regolith is a silty soil with particles less than 1 mm in diameter [5]. Complex natural comminution (destruction) and agglutination (creation) processes throughout geologic time determine the size, shape, and content of the regolith material. The particle size distribution of lunar soil is shown in Figure 3.5. The particle size's do not differ significantly between the mare soils, the highland soils, and the mare-highland interface [11]. However, there are some compositions distinctions with particle size. This might be beneficial for more global design purposes.

For testing purposes since a genuine lunar regolith is not available, **Lunar Highlands Simulant-1**[12] is used. In Chapter 4 the validity of using simulant instead of genuine regolith for testing purposes is discussed. The lunar dust simulant (LHS-1 Lunar Dust) [12] has the properties listed in the Table 3.1. The dust is also reflective and may conduct light. The particle diameter distributed is shown in Table 3.5.

Table 3.1: Small overview of simulant properties adapted from [12]

Parameter	Value	Unit
Uncompressed Bulk Density	1.30	g/cm^3
Grain Density	2.75	g/cm^3
Mean Particle Size	90	μm
Median Particle Size	60	μm
Particle Size Range	<0.04 - 1000	μm

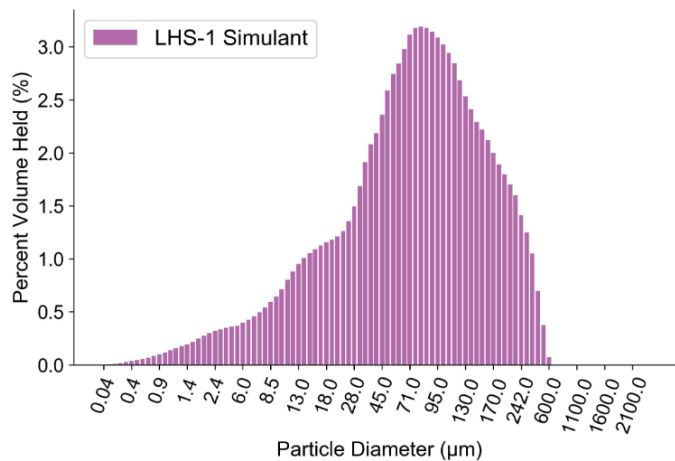


Figure 3.5: Percent Volume by Particle Diameter from spec sheet [12]

Table 3.2: Relative dielectric constant and density of particles of common materials in lunar dust simulant [12]

Oxide	Wt. %	Density	Relative dielectric constant
SiO_2	51.2	2,65 g/cm ³	3.7-3.9
Al_2O_3	26.6	3,95 g/cm ³	9.9
CaO	12.8	3,34 g/cm ³	11.8
Na_2O	2.9	2,27 g/cm ³	
FeO	2.7	5,745 g/cm ³	14.2
MgO	1.6	3,58 g/cm ³	9.7
TiO_2	0.6	4,23 g/cm ³	85
K_2O	0.5		
LOI	0.4		
P_2O	0.1		
MnO	0.1	5.026 g/cm ³	9.7

3.2.1. Particle deposition on rover

Lunar dust lofting is the most commonly accepted theory for explaining the Lunar Horizon Glow (LHG), which is a phenomenon in which a glowing beam is seen near the moon's horizon. Charged dust particles could be lofted due to electrostatic forces and consequently transported due to the potential difference between the day and the night sides of the moon. In this [13] study, the maximum heights of the dust particles with 0.1, 1 and 5 micrometer radius are estimated for the three different coronal mass ejection events together with the lunar surface potential, electric field, Debye length, and the location of the dead zone. The intensity of dust differs throughout the night and day. The theoretical height of a **5 micrometer** particle is between **15 and 50 cm**. In [4], it is mentioned that the estimates for the dust particle concentration differ by several order of magnitudes. It should also be noted that all of these models are based on sightings and known particle properties.

Micrometeoroids are another reason for particles becoming airborne, is the impact of micrometeoroids on the lunar surfaces. In [14], a thorough analysis is provided of the lunar dust environment, including the impact of interplanetary micrometeoroids on the Moon, the crater record, and the soil characteristics. In addition to discussing novel lunar dust transport hypotheses and experiments, this paper sheds light on possible lunar surface processes. The report emphasizes that approximately 106 kg of interplanetary micrometeoroids of cometary and asteroid origin bombard the Moon annually. Most of these projectiles range in size from 10 nanometers to 1 millimeter and impact the Moon at velocities between 10 and 72 kilometers per hour. There is a significant flux of secondary sub-micrometer-sized ejecta particles generated by interplanetary meteoroids at the lunar surface. Similar ejecta clouds have been observed surrounding all of Jupiter's Galilean moons. In addition, the paper emphasizes outstanding issues in understanding the lunar dust environment as well as future missions and experiments designed to address these issues. Overall, this report is a valuable resource for researchers

wishing to comprehend the intricate dynamics of the lunar dust environment.

Another source of deposition could be **human activity**. Either the rover itself or other rovers could propel dust onto the solar panel. In [15] a model was made for a solar panel that was within 1 kilometer of a landing site. For 10 launches and landings of a vehicle with a maximum thrust of 26,800N, the resulting $2mg/cm^2$ deposit would result in a loss of power of around 35%.

As mentioned before, there are many models for dust lofting, which differ by several orders of magnitude. It is also unclear how much of this particle concentration actually deposits on the lunar surface. The only in situ experiment that collected information about particle deposition was the Lunar Ejecta and Meteorites (LEAM) experiment. In [17] this experiment is interpreted, and the conclusion is drawn that '**the LEAM events** which are measurements made by the detector and are consistent with the sunrise/sunset-triggered levitation and transport of slow moving, highly charged lunar dust particles.' It is also mentioned that the rapid decline of events on the up sensor might be due to an accumulation of dust. The number of events per day before this decline was around 40. Combined with the sensor area of $100cm^2$ [16], **this results in 4000 'impacts' per day per m^2** . It should be noted that the amount of data gathered from this experiment is limited, that it was performed over 50 years ago, and that the experiment was not even setup for registering dust particles, but to detect **hypervelocity** impacts. Using the calculations for maximum height of dust lofting, the approximation is made that the dust that lands on the rover from natural phenomena is most likely **below 100 micrometer in size**.



Figure 3.6: The LEAM detector unit, from [16]. On top the detector that measured the relevant data.

3.3. Effect of lunar dust on the efficiency of solar panels

The efficiency of a solar panel is determined by many fundamental criteria, including the highest possible efficiency and the maximum voltage per cell, which corresponds to the maximum current. On the other hand, the amount of radiation received by photovoltaic cells is a critical predictor of efficiency and can be directly altered by obstacles such as dust particles.

3.3.1. Theoretical Analysis

Bouguer-Lambert law relates the light intensity loss due to a medium. This is used to calculate the transmission loss of solar irradiance due to dust buildup. [18] Bouguer-Lambert law is given by the following equation:

$$\frac{I}{I_0} = e^{-NA_p Q_{ext}} \quad (3.1)$$

where I is the light intensity incident on the solar collector after it has passed through the dust layer, I_0 is the light intensity incident on the solar collector when it is completely clean with no deposited dust particles, N is the number of deposited particles per unit area, and A_p is the projected surface area of a dust particle, calculated as $A_p = (d/2)^2\pi$ for a spherical particle with diameter d . A visual representation of these parameters are shown in Figure 3.7. The extinction effectiveness of a particle, indicated as Q_{ext} , is the total of its scattering and absorption losses, denoted as Q_{sc} and Q_{ab} , respectively. Q_{sc} is determined by the ratio d/λ , where λ is the wavelength of irradiance. There are estimate value for Q_{ext} described in [18] these values are estimated to be around 2.5-3.5. This value assumes linear absorption and no dependency of the wavelength λ . For further analysis a average value of 3 is used.

3.3.2. Experimental Analysis

Because of the dry lunar atmosphere, experiments have been done to imitate the lunar environment and analyze the influence of dust on the solar panels. To more completely mimic lunar conditions and hence the effect of dust deposition, a very dry test bed must be built. A test room featuring a sun filter, a humidity control system, and a dust deposit system was developed in the work of [19].

This tests have been performed with both lunar and martian dust in the [19]. Figures A.1, A.2, A.3 and A.4 show the results for voltage current and power of solar panel per deposited dust mass for lunar

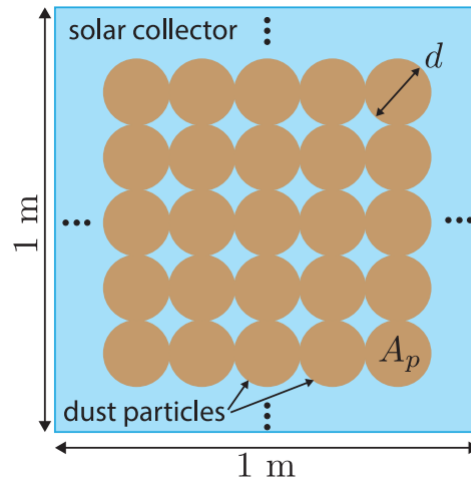


Figure 3.7: Figure for dust particles adapted from [18]

dust.

3.4. Electric field and Breakdown

Breakdown is a phenomenon in which the dielectric material is unable to withstand the applied electrical stress, resulting in a sudden and significant increase in current flow. This breakdown can occur due to various factors such as high voltage, excessive temperature, or the presence of impurities or defects within the material. In general this process starts when the first electron hits the other side of the electrode. This initializes a feedback process that creates more electrons that jump into the gap. [20] **Paschen's law** describes the relation between the breakdown voltage and the gas pressure. Its important to make this into account as due to the reduction in the breakdown voltage following Equation 3.2] there is a need to have a suitable vacuum intensity during a vacuum test; else, breakdown occur. Paschen's law is described by the formula below.

$$V_b = \frac{Bpd}{\ln(Apd) - \ln\left[\ln\left(1 + \frac{1}{\gamma_{se}}\right)\right]} \quad (3.2)$$

Where V_b is the breakdown voltage (V), p is the pressure in pascal (Pa), d is the gap in meters (m), γ_{se} is the secondary electron emission coefficient which takes into consideration secondary emission of particles after an initial event has happened. A is the saturation ionization in the gas at a particular $\frac{E}{p}$ and B is related to the excitation and ionization energies. The important takeaway from the Equation 3.2 is that the atmosphere on the moon, notably the vacuum intensity, is adequate to imply that the breakdown threshold is not a concern.

Nerveless due to the test condition on earth its important to characterise the breakdown voltage. The dielectric strength of air is $E = 25kv/cm$, which is the same as $E = 2.5kv/mm$. After reaching this electric field strength, ionization of air starts to take place. This is called corona.

3.4.1. Field electron emission

This is a phenomenon in which electrons are released from the surface because of the high electric field strength. For short gaps under 2mm it is the most dominant breakdown effect that occurs with a field strength of 20 to 30 kV/mm [20]. This effect occurs for weak conduction or nonconducting dielectrics. Field emission is described by quantum mechanics and its done by the Fowler-Nordheim equations. Heating the electrodes has an effect on the field strength needed to observe field electron emission. This is called heat emission. This is also modeled by the Fowler-Nordheim equations[20].

Because the system described in this thesis does not concern these high field strengths. Its not going further into depth. But this equation gives an absolute maximum field strength for space applications.

3.4.2. Dielectric barrier discharge

Dielectric barrier creates gaseous ions and electrons which are driven to one side of each electrode. This charges the natural charged particles much higher[21]. This method requires an atmosphere or any other material.

The substrate where the electrodes are placed up on which is primarily glass. has a dielectric break-down between $10 - 30\text{kV m m}^{-1}$. This is far greater than that of air. That is why breakdown for the substrate is not further discussed in this thesis.

3.4.3. Field Enhancement

Field enhancement is a phenomenon in which the electric field strength is increased locally because of the shape of the electrode [22, 23]. The effective electric field is described by the following relation:

$$E_m = \beta E \quad (3.3)$$

Where β is the field enhancement factor. This enhancement for some geometries can be seen in Figure 3.8.

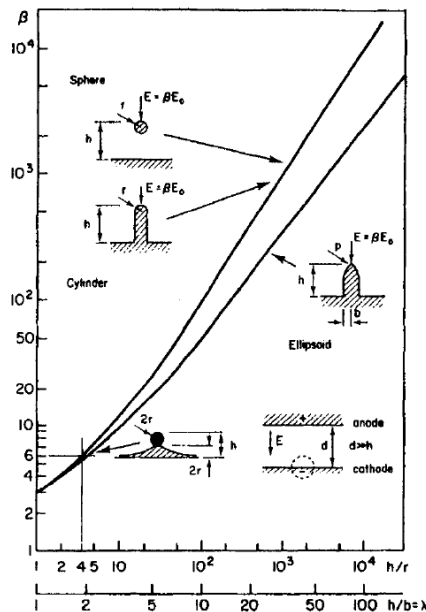


Figure 3.8: Field enhancement factor β from [23] with $b = w/2$

3.5. Dust particle model

Dust particles experience various effects when placed on the EDS system. Its important to characterize these effects for future modeling of and optimization of an EDS system. It also provides a basis for understanding the phenomena. We will start by describing gravity.

3.5.1. Gravity

The gravitational constant on the Moon is around $1,62\text{m s}^{-2}$ which is much less than on earth. Gravity plays an important role in dust-lofting on the Moon that why it is mentioned here [13].

The gravity on a spherical particle is described by the following Equation [24]:

$$F_{\text{grav}} = \frac{1}{6}\pi d^3 \rho g_s \quad (3.4)$$

With radius r_d , density ρ and g_s as the gravitational constant.

3.5.2. Air drag

Another force experienced by dust particles on the earth is the drag force. This force is due to air friction and can be mathematically described by the following equation:

$$F_D = \frac{1}{\tau_p} m_p (u - v) \quad (3.5)$$

where u is the air velocity in meter per second (m s^{-1}), v is the velocity (m s^{-1}) of the particle and m_p the mass of a particle in kilo grams (kg). $\frac{1}{\tau_p}$ is the drag coefficient [25] defined by:

$$\tau_p = \frac{\rho_p d_p^2}{18\mu} \quad (3.6)$$

Because there is no atmosphere on the Moon this force is not considered in further analysis. Its listed here because when the experiments are conducted on Earth, the force is considerable and cannot be neglected [25]. The drag coefficient is defined as : Where ρ_p is the particle density and d_p is the particle diameter in m.

3.5.3. Particle electrostatic forces

The dominant driving force exerted on a particle when placed on a EDS screen is the **Lorentz force law**. Lorentz force law is described by the following equation. [24]:

$$\vec{F} = q(\vec{E} + \vec{v} \times \vec{B}) \quad (3.7)$$

There is no significant presence of an magnetic field (\vec{B}) then by rewriting it results in the equation for **Coulomb force** which is defined as:

$$\vec{F}_c = Q\vec{E} \quad (3.8)$$

Where \vec{F}_c is the force vector, Q is the particle charge and \vec{E} is the electric field vector.

The charge on a particle assuming that a particle's charge distribution is uniform, Gauss law will describe the electric field and charge as follows: [24]

$$Q = E_p A \epsilon_0 \quad (3.9)$$

Where E_p is the electric field produced by the particle, A is the surface area and ϵ is the permittivity constant. **The electrical conductivity** of unirradiated lunar soil can be as low as 10^{-14}S/m [26]. In Figures 9.50 and 9.51 of [11] it can be seen that for the same temperature this conductivity starts to increase significantly when irradiated, up to a factor of 10^6 . This is noticeable because the particles that will settle on the solar panel may have been irradiated for some time. The low conductivity means that the particles can easily be charged. In [27], Mars simulant and silica microspheres were charged by exposure to three different conditions: (a) thermal plasma and electron beam, (b) electron beam, and (c) UV radiation. For this irregular-shaped Mars simulant ranging from $38 - 45 \mu\text{m}$ in diameter, a charge between $1 - 1.5 \cdot 10^5 e$ was found. Additionally, it was seen that the charges on approximately equal-sized single particles can also have large variations due to the variations in shape and size of the microcavities in which highly varied electric fields on the surfaces of the surrounding particles are created.

Other mechanisms for particles to get charged exist. Tribocharging is one of these, which will be explained in Section 3.5.6. This charging effect has the potential to attract non-charged particles to surfaces of the solar panel. This effect is important for dust removal because it can induce charges on non charged particles.

3.5.4. Adhesion and Cohesion in Electrostatic Lofting

Adhesion force is an abstract phenomenon that occurs on the surface of the solar panel. This consist mainly of Waals forces, capillary forces, chemical and mechanical [25]. [21]

From [24] [21], one may conclude that cohesion between the particles also plays a central role. This phenomenon is largely due to Coulomb's forces described by single particles in the following equation. [25]. Form the paper[28] we can drive the formula as follows for the cohesion force.

$$F_{co} = \frac{-D}{48(t+d)^2} \frac{r_1 r_2}{r_1 + r_2} \quad (3.10)$$

Here the assumption is for two spherical particles with radius r_1 and r_2 . D is the **Hamkar constant** with a small explanation in appendix A.2. It describes the body-to-body interaction of van der Waals forces, for powder, this is roughly $(4.3 \cdot 10^{-20})$ Joules for lunar soil [28]. It is the minimum distance between the particle and the surface due to the absorbed molecules and d is the distance between the particle surface $\frac{r_1 r_2}{r_1 + r_2}$ approaching the radius of a dust particle so r_d . By substitution of S, the approximate cleanliness of the granular powder defined as $S = \frac{B}{t}$ [29] where B is the diameter of the O^{-2} ion ($B = 1.32 \cdot 10^{-10}$) the following simplified equation is obtained.

$$F_{co} = -CS^2 r_d \quad (3.11)$$

S for lunar surface is 0.75 at night and 0.88 during the day [28]. and $C = 5.14 \cdot 10^{-2} \frac{kg}{s^2}$. This is result can be extended for the case of a flat surface and a particle where on can write:

3.5.5. Dielectrophoresis

Dielectrophoresis (DEP) is a phenomenon in which a force is exerted on a dielectric particle when it is subjected to a **non-uniform electric field**. Particles are attracted to regions of stronger electric field when their permittivity ϵ_2 exceeds that of the suspension medium ϵ_1 , that is, when $\epsilon_2 > \epsilon_1$. Particles are repelled from regions of stronger electric field when $\epsilon_2 < \epsilon_1$. [30]. It is also noteworthy to mention that the Dielectrophoresis forces are much weaker than the Lorentz force. The DEP forces acting on a lossless spherical particle are related with the following equation [30] :

$$\vec{F}_{DEP} = 2\pi\epsilon_1 R^3 K \nabla E_0^2 \quad (3.12)$$

Where \vec{F}_{DEP} is the force exerted on the particle in newtons, ϵ is the permittivity of the medium where the particle is in suspended, ϵ_2 is the permittivity of the particle, R is the radius of the particle, E_0 is the applied electric field and K is the **Clausius-Mossotti function** K given which expresses the dielectric constant to the atomic polarizability by the following equation:

$$K = \frac{\epsilon_2 - \epsilon_1}{\epsilon_2 + \epsilon_1} \quad (3.13)$$

3.5.6. Tribocharging

Due to the effect of dielectrophoresis, another physics effect plays a role in dust removal. Because the DEP forces are pointing in the direction of the electrodes, friction forces generate charges on un-charged particles. Then after charging the strong Coulomb forces will push the particles away.

The build-up charge depends on the surface roughness, temperature, strain, and other properties.

Tribocharging of lunar dust is a difficult phenomenon and has not been modeled before. Its only done experimentally. A recent paper in May 2023 claims that tribocharging should be studied better in various exploration scenarios [31]. Experiments done by [32] states that the **tribocharging effect** charges the particles to around $0.01\mu C g^{-1} - 0.03\mu C g^{-1}$.

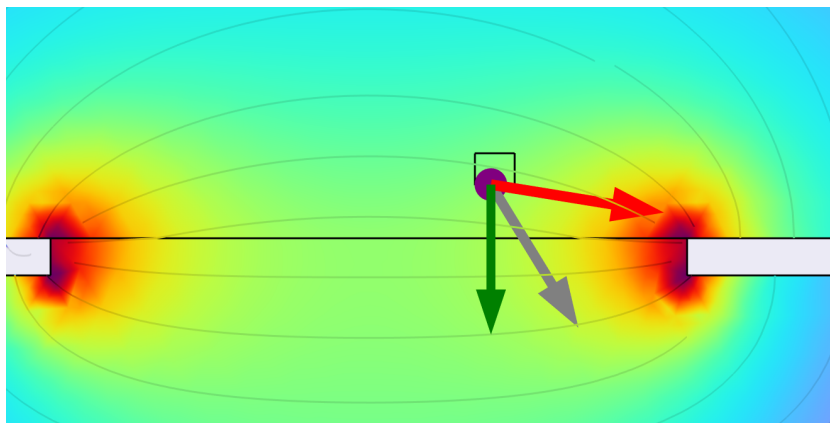


Figure 3.9: An overview of the forces and their direction in the Electric field of a typical EDS system. The color of the arrows corresponds to the following forces: Red = Coulomb, Gray = DEP, Green = Gravity

3.6. Friction and static clinging

The last part of the analysis of the force is dedicated to the **friction** and **static clinging**. Due to statically charged particles dust will cling to a surface the same way. The friction forces are described as follows.

$$F_f \leq \mu F_n \quad (3.14)$$

Where F_f is the force of friction exerted direction opposite to the travel direction μ is the friction coefficient depending on the material F_n is the normal force. This is mainly due to gravity.

An overview of some forces are shown in Figure 3.9.

3.7. Conclusion and model of dust particles

After this background study on dust particles, a model can be made of the properties the dust particles relevant for removal. These are summarized in the following table:

Table 3.3: Particle range of interest to be used in design equations

	LHS-1 Simulant
Particle Diameter	$1\mu m - 100\mu m$
Average particle diameter	$50\mu m$
% mass of LH1-Simulant	52.7%
Grain density	$2.75g/cm^3$
Primarily substances	SiO_2, Al_2O_3, CaO
Electrical conductivity	$10^{-14}S/m - 10^{-7}S/m$
Number of particles depositing on rover	$4000/m^2/day$
Estimate charged due to tribocharging [32]	$0.01\mu Cg^{-1} - 0.03\mu Cg^{-1}$
Average particle mass	$31\mu g$

Due to a maximum particle diameter of $100\mu m$ all particles under $100\mu m$ are chosen, resulting in a 52.7% of the mass of lunar dust. The particle diameter is estimated with the data provided from [12] This results to a particle size of $50\mu g$ Its important for further estimation to establish a minimum particle diameter. The absolute minimum for this analysis is chosen to be around $1\mu m$. Furthermore, it is assumed that the particles that end up in the solar panel are mainly consistent with the following three materials SiO_2, Al_2O_3, CaO .

4

State of the Art

This chapter gives an overview of the findings in previous research. Discussed are different architectures and signals for driving these architectures. The validity of testing setups and usage of FEM modelling software is also assessed.

4.1. Design parameters

The first step of creating an EDS is determining what architecture to use. Most commonly used [33–35] is a straight parallel design. This has the advantage of being easier to fabricate, and has a less complex electric field. Other designs are also used. In [36] it was found that for their experiment setup, a zigzag electrode design removed more dust and worked faster than a parallel design. Another possible design is a spiral, for which variants are tested in [37]. This design was used to ensure there exists no overlap between electrodes for a multiphase design, such that the manufacturing can be done for a two-dimensional configuration. An visual overview of these designs can be seen in Appendix B.1.2. It must be noted that the results of the experiments can be hard to compare, since there is a lot of variation in test setups and electrode manufacturing.

Most EDS systems use a three- or four-phase traveling wave [34, 36, 38], in which the electrodes are driven by a delayed AC signal in a particular direction. [35] explains that the difference between the traveling wave and a standing wave is that 'both repel from the electrode array, but the latter provide lateral translation along the array.'. In [21] it is mentioned that removal can be seen for both forms of supply. The standing wave is used in [33] and [39]. In [39] the supply voltage is in the same range as the traveling wave systems, but there is no information on the geometry, so no comparison on effectiveness can be made. In the standing wave system of [33] a significantly higher voltage is required for removal. This supply voltage is perhaps one of the most important parameters, as this directly impacts the electric field, which impacts the forces driving the removal. Increasing the voltage increases the removal efficiency [37][40]. In the latter, the voltage threshold for any removal is found to be 400V, which is due to adhesion forces. This threshold value was also found in [41] for a relative humidity below 55%.

The type of AC signal is another aspect that can be varied. The first is the frequency, for which an optimal removal rate is found between 5-50 Hz, which depends on the size and type of material removed[36, 42]. In [42] and [40] the removal efficiency is reduced for higher fre-

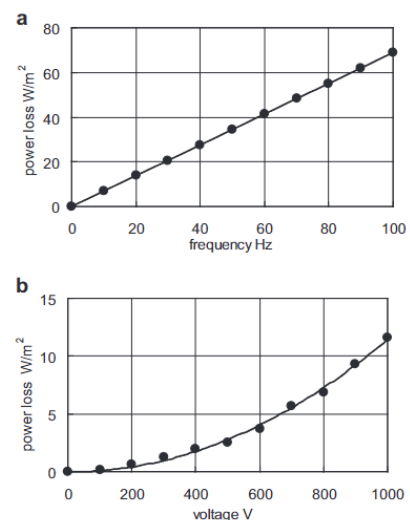


Figure 4.1: (a) Power loss with respect to frequency (800 V). (b) Power loss with respect to applied voltage (10 Hz). From [37]

quencies, and in [40] the particles only vibrate for frequency over 300Hz. The frequency does not only impact the removal efficiency, but also the power usage. In [34] the power consumption increased with frequency, which is explained by considering the EDS as a capacitive load. In [37] this linear power loss increase with frequency is also seen. The second is the type of signal supplied. [40] tested particle removal for triangular, rectangular, and sinusoidal waveforms and found that the amount of particles not transported at any frequency is the lowest for rectangular. [42] found rectangular to be the best performing waveform too, and reasons that the steeper signal growth is responsible. This seems plausible, since that way a particle should more quickly receive more Coulomb Force (Section 3.5.3) which results in a higher final velocity.

Most experiments focus only on the removal of dust and use PCBs for easier manufacturing. This is understandable but means that there is no information about the impact such a system has on the surface below, such as a solar panel. In [34] the electrodes are etched onto a ITO-coated PET substrate, which resulted in a power loss between 13.7% and 16.3% for the solar cells of an EDS system with electrodes covering 1/11th of the cells.

4.2. Removal Mechanism

The mechanism of removal is discussed in some of the research. In [39] the particles were seen moving side to side which is explained with the effect of DEP forces. Another interesting finding [37] is that initially charged dust was removed more quickly, but that the eventual removal rate was not impacted by the initial charge. This suggests some effect takes place that either charges the particles or that the removal of particles is not impacted by charge. In [35] the removal mechanism is explained as follows: "As DEP attracted particles towards regions of greater field strength, the particle itself would locally distort the field further, intensifying it to the point of triggering electrostatic repulsion."

4.3. Testing and Simulation

Creating a test environment that fully simulates the lunar surface is complex. Therefore, it is important to know what the impact is of the limitations a test setup might have. The lack of an atmosphere makes a big difference [37]. A reasoning given for the higher removal efficiency obtained in this experiment for a vacuum is the lack of air containing moisture, which causes agglomeration. In [41] this decrease of removal efficiency for an increase in relative humidity was experimentally confirmed. This is probably also the reason that experiments such as [34] first dry their test material. The test material used is another limitation, as there is a sparse amount of actual lunar soil available on Earth. In [37], the same EDS system is tested for both a lunar soil simulant as real lunar dust. More real lunar dust was removed, from which was concluded that using simulants for testing is a conservative approach in testing removal performance.

Several papers use FEM modeling, mostly for solving the electric field of complex electrode designs. The finite element method is a method of splitting models into smaller elements (meshing) so that the system can be solved numerically. There is also research [42, 43] that models the particle trajectories, but these make two major assumptions. The first is that the particles retain a constant charge during the simulation. The second is the lack of adhesion forces between the particle and the surface, which will play an important role in determining our design parameters. Another assumption is the lack of particle-particle interaction, which will be shown to have an impact when the system is loaded with a large number of particles. In [40] it is experimentally shown that the simulations of single particles do not conform to the experimental results. The issue of fixed charges is also noted as a limitation of simulation methods in [44].

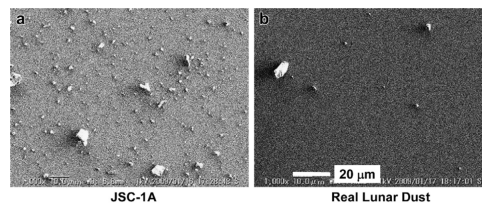


Figure 4.2: Residual dust after cleaning operation. From [37]

5

Electrodynamic Screen model

After conducting a thorough trade-off analysis and literature review, it has become clear which design choice should be made for the EDS system. This leads to the question of how the EDS electrodes should be designed in order to generate the necessary electric field and effectively eliminate dust particles from the screen. In this chapter, we will present the model of the EDS system, focussing particularly on the impact of electrode design on particles.

5.1. Electrode Architecture

In a simplified model, each pair of electrodes in the EDS system can be viewed as a capacitor. When a charged particle is subjected to a force, denoted $\vec{F} = q\vec{E}$, it begins to move within the electric field. As the particle gains sufficient momentum, due to phase change the electrodes change polarity, causing the particle to continue its movement and be removed from the screen.

This forms the foundation of the initial design, where, for the sake of simplicity, the architecture consists of parallel straight electrodes. In this design, each set of three adjacent electrodes is continuously supplied with a three-phase supply. Henceforth, this design is referred to as the **parallel architecture**. Thanks to the relative simplicity of this architecture, it becomes feasible with simplifications to solve the electric field analytically and in a closed form. [45]

Another option to improve the electric field is to incorporate sharp corners in a design known as a **zigzag** architecture. Based on the effect of field enhancement, which is explained in section 3.4.3, it is anticipated that the electric field will be amplified at the same voltage level by the sharp corners. This enhancement in the electric field (especially) in the y-direction is expected to facilitate greater removal of dust particles from the screen. But at the same time, it will make the breakdown far more likely

The third architecture, known as the **spiral design**, has been used in the reports of NASA and ESA. In this design, the trajectory of dust particles is anticipated to be centrifugal rather than linear. Our team has also conducted tests that incorporate this design into the experimental setup. However, due to the complexity of analytically solving the electric field for such an architecture, we only mention it without delving into further details.

There are still numerous uncertainties surrounding the electrode architecture and many possible creative options. In a study conducted by [46], they used an experimental approach based on trial and error to investigate this matter. However, since the focus of this report is to assess the feasibility of TRL 3 and 4, exploration beyond trial and error has been restricted to the zigzag and parallel architectures. The aim is to gain a deeper understanding of the behavior of EDS systems and modeling of it.

5.1.1. Orientation of Electrodes

Two primary orientations for electrode placement are considered in the rover: horizontal and vertical placement. The decision has been made to position the electrodes in a vertical orientation (Figure 5.1b).



(a) Horizontal electrode orientation

(b) Vertical electrode orientation

Figure 5.1: Possible Electrode orientations

This choice is based on two factors: the front-facing camera vision of the rover and the presence of a mechanical solar panel tilt mechanism at the back. These areas are particularly vulnerable to stresses caused by lunar dust and potential visual obstruction. Based on this reasoning, it can be concluded that the length of the electrodes is approximately equal to the length of the panel, which measures approximately 32 cm.

5.2. Design parameters

The optimization of an EDS design can be carried out considering various parameters below. By modifying these parameters, different electric field characteristics can be generated, leading to a significant impact on the movement of particles and whether they can be effectively removed from the panel.

- w Width of the electrode
- p Pitch between the electrodes
- f Frequency of applied square wave
- ϵ_2 Dielectric permittivity of the base material
- s Spacing to ground plane

For the **zigzag** electrode design, there are additional parameters which are shown in Figure 5.2. These are

- a is the angle between the legs of the zigzag elements.
- h is the height of the triangle
- $Unit_{length}$ is the length of a zigzag element, which follows from the angle and height.

To implement these patterns, automation through code is employed, as described in the following: B.1. Using this approach, it became feasible to efficiently design the same architecture with different parameters.

The pitch p and width w are difficult parameters to define. In most research papers they make educated guesses on these parameters or test multiple ones [37]. The widely used spacing is 0.3 mm width and 0.6 mm pitch. This will also be the basis for the experiments done in Chapter 6.

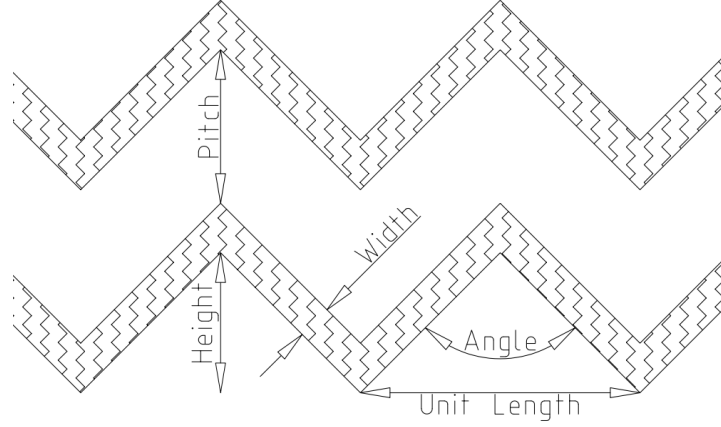


Figure 5.2: Zigzag parameters

5.3. Transmission model

Because the electrodes have a high voltage applied to them and are sufficiently small. It may be important to consider transmission phenomena. First, its important to consider the highest switching frequency. By digitally construction of a PWM switching frequency of 500 Hz seen in Figure 5.3a and doing a frequency analysis which is plotted in Figure 5.3b

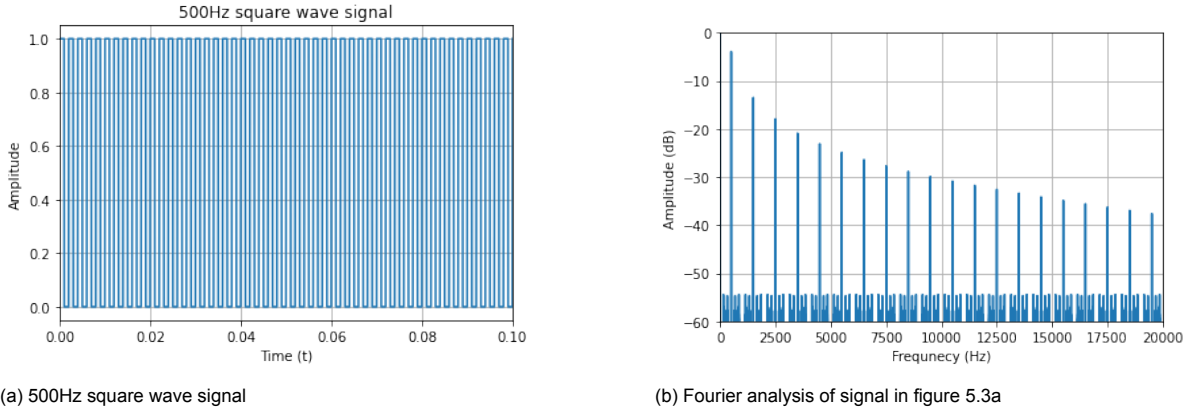


Figure 5.3: Comparison of signal and its Fourier analysis

The 99% percent power band width is calculated to be around 6400hz. We take this to be the highest frequency component. Taking this frequency and putting it in the boundary equation for consideration of electromagnetic propagation given in [47].

$$\frac{l}{\lambda} \geq 0.01 \quad (5.1)$$

with lambda defined as $\lambda = \frac{u_p}{f}$. This results in the following equation:

$$\frac{\sqrt{\epsilon_r} \cdot l \cdot f}{c} \geq 0.01 \quad (5.2)$$

Filling in gives a value of $3.3e - 06$ which is much smaller than 0.01. However, it may be important because the transmission is determined by the following equation.

$$\frac{V(\omega)}{A} = e^{-\sqrt{R'j\omega C'} \cdot l} \quad (5.3)$$

Equation 5.3 is derived in Section A.6. When the electrode area becomes small, the resistance of the electrode becomes significant high. This will influence the transmission.

5.4. Breakdown

Breakdown occurs when the electrical field strength is greater than the dielectric strength of the insulator. For an insulator of air this is 25kV/cm. Because of Paschen's law described in Section 3.4 which relates the atmospheric pressure and the breakdown voltage. In vacuum conditions the dielectric breakdown voltage is sufficiently high that this is not the dominant. Without any protective coating on the electrodes dust bridges may create breakdown. The lunar dust mainly contains insulating materials which are summarized in Table 3.2. Breakdown will not be considered as a potential problem of dust removal system. The applied voltage largely depends on the implementation of inverter and the materials insulating it. Higher potentials are preferred.

5.5. Equivalent capacitance

To obtain a comprehensive understanding of an electrodynamic screen, it is crucial to develop an equivalent electrical model. In the case of the electrodes, this model primarily includes a capacitive element. The analytical expression for the coplanar capacitance is rather hard. The capacitance between two plates can be found by evaluating the integral given in Equation A.9. Evaluating this integral becomes rather tedious.

To fix this problem a rather simple simplification can be used namely the parallel line capacitance model which is given by Equation A.16. The only problem is that the spacing between the two conductors are equivalent to the width of the electrodes. This model is not valid anymore for this specific application. That's why another model is used proposed by R. Zypman [48]. This is rather a difficult equation that utilizes some advanced mathematical tools. The full explanation and evaluation of the equation is given in Section A.6.3.

To show the difference between the parallel line model and that of R. Zypman [48]. The following plot is constructed seen in Figure 5.4.

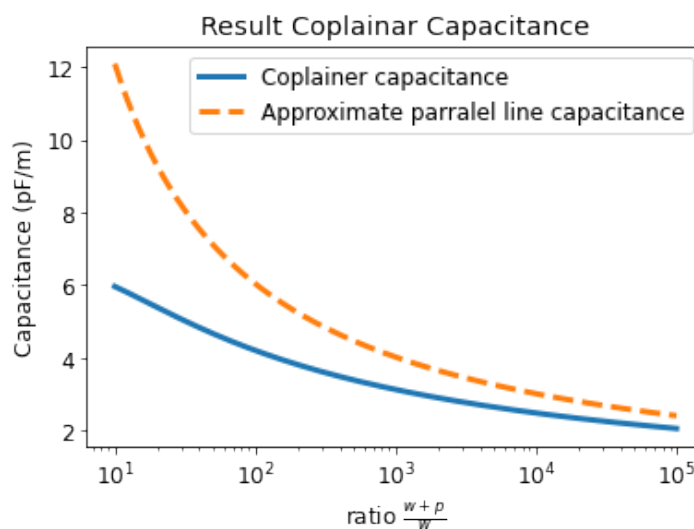


Figure 5.4: Coplainer capacitance vs parallel line capacitance

5.6. Simplification of Electric field

Modeling the electric field of an EDS system is important since it allows a prediction of the behavior of the particles at the top of the panel. It can be used to determine the impact of various parameters on the system, such as the electrode size and shape, the material type, and the voltage applied. It can be used to identify its effects. Furthermore, models can be used to optimize system design for specific applications. In this section, the derivation of a simple electric field model is explained.

The model proposed in this thesis starts with two charge distributions which have a width of w and spacing between them with pitch p . These two have an equivalent charge of Q and a respective charge density of $\rho_Q = \frac{Q}{2 \cdot w}$. p_n is the observation point of the electric field, and x is used for integration and evaluation.

Now that the charge density is defined, the electric field can be evaluated using the equation A.5.

$$\vec{dE} = \left[\begin{array}{c} \frac{q(p_x - x)}{8\pi w \epsilon (p_y^2 + |p_x - x|^2)^{\frac{3}{2}}} \\ \frac{p_y q}{8\pi w \epsilon (p_y^2 + |p_x - x|^2)^{\frac{3}{2}}} \end{array} \right] \quad (5.4)$$

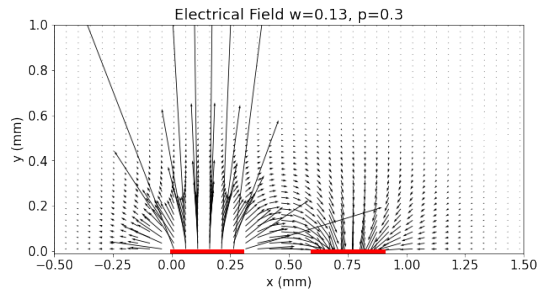
After evaluating the indefinite integrals the result is shown in the following equation

$$\int \vec{dE} = \vec{E} = \left[\begin{array}{c} \frac{q}{8\pi w \epsilon \sqrt{p_x^2 - 2p_x x + p_y^2 + x^2}} \\ \frac{q(-p_x + x)}{8\pi p_y w \epsilon \sqrt{p_y^2 + (p_x - x)^2}} \end{array} \right] \quad (5.5)$$

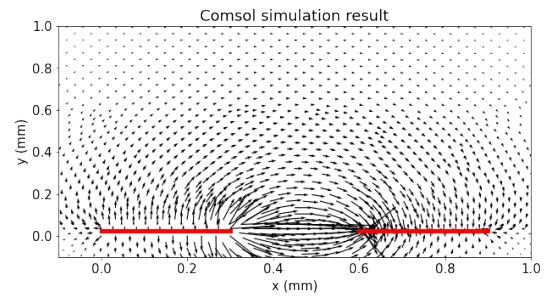
To make this integral definite, we should evaluate the integral from 0 to w and any other electrode. In this case, from $w + g$ to $2w + g$. After evaluation, the electric field can be written in the form of:

$$E(p_x, p_y) = \left[\begin{array}{c} -\frac{q}{8\pi w \epsilon \sqrt{p_x^2 - 2p_x(g+2w) + p_y^2 + (g+2w)^2}} + \frac{q}{8\pi w \epsilon \sqrt{p_x^2 - 2p_x(g+w) + p_y^2 + (g+w)^2}} + \frac{q}{8\pi w \epsilon \sqrt{p_x^2 - 2p_x w + p_y^2 + w^2}} - \frac{q}{8\pi w \epsilon \sqrt{p_x^2 + p_y^2}} \\ \frac{p_x q}{8\pi p_y w \epsilon \sqrt{p_x^2 + p_y^2}} + \frac{q(-p_x + w)}{8\pi p_y w \epsilon \sqrt{p_y^2 + (p_x - w)^2}} + \frac{q(g - p_x + w)}{8\pi p_y w \epsilon \sqrt{p_y^2 + (-g + p_x - w)^2}} - \frac{q(g - p_x + 2w)}{8\pi p_y w \epsilon \sqrt{p_y^2 + (-g + p_x - 2w)^2}} \end{array} \right] \quad (5.6)$$

Evaluating this equation using python with Numpy[49] for a pitch and with of 0.13 mm and 0.3 mm correspondingly the following figure can be constructed:



(a) Electric vector field due to a positively and negatively line charge distribution (red).



(b) Electric vector field constructed using COMSOL[50]

Figure 5.5: Constructed Electric vector fields

In Figure 5.5a it can be seen that the electric field strength will approximate infinity when the electrode surface is reached. Using COMSOL [50] the same is done, but now numerically. This results in the vector field given in Figure 5.5b.

5.6.1. Comparing and fitting to COMSOL

Because the constructed electric field in Equation 5.6 assumes that the charge distribution is uniform. From simulations done in COMSOL simulations this may not be the case. Never less, it can may numerically approximate the electric field. Therefore, different pitches are compared to the numerical simulation.

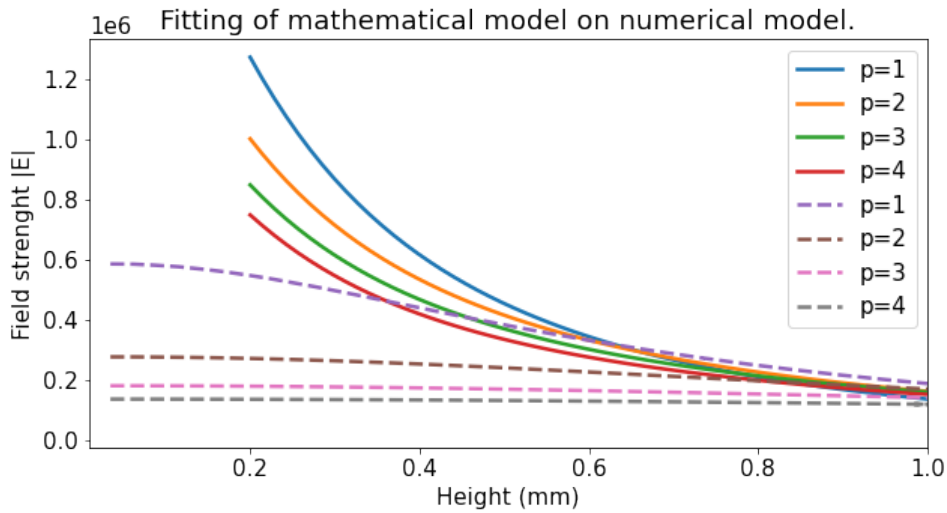


Figure 5.6: Electric field norm $|E|$ in the middle between the electrodes. Solid line Mathematical model given by equation 5.6. Dashed lines: Comsol simulation result.

In Figure 5.6 the numerical simulation (dashed lines) are compared with that of the constructed mathematical model given by Equation 5.6 (solid lines). After fitting of the charge parameter the results shows that the mathematical model does not predict the electric field strength enough under 0.6mm . But for farther distances, it gives an estimate.

5.7. DEP forces

Now that there is some sort of simplified mathematical solution to the two-line electric field charges. The DEP forces can be calculated using formula 3.12. Due to the complexity of equating the gradient of the above electric field in Equation 5.6, a symbolic mathematics package of Python [51] is used, this is called Sympy [52].

The Clausius-Mossotti function in Equation 3.13 will always give a positive result. The result due to the relative permittivity of any of the dust particles is higher than that of vacuum. After evaluation of the DEP force equation, the following plots is constructed:

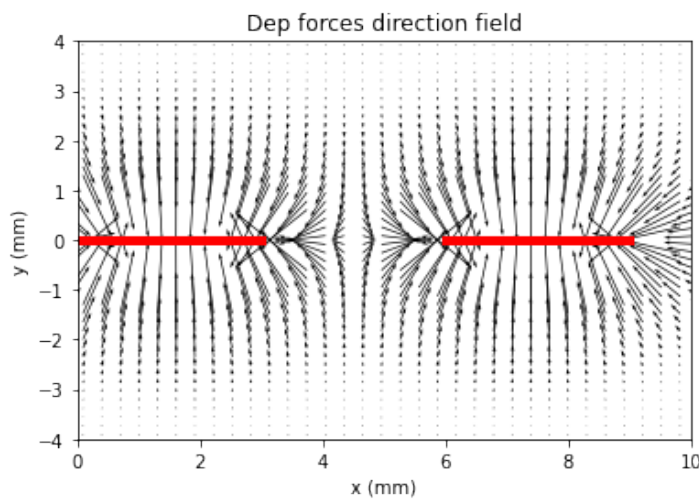


Figure 5.7: Visual representation of the DEP force vector field

The DEP forces are in the direction of the electrodes. This verifies the statement that Dielectrophoresis (DEP) is not the main phenomena for removing of dust. Because otherwise the dust will be even more adhesive to the electrodes. Its also important to see that the DEP force precisely in the middle of the two electrodes is zero due to the symmetry of the problem. This means that there may be a possible accumulation of dust since no particles are charged there.

5.8. Particle force model

A force model is important for dust modeling of an EDS system because it allows for prediction and simulation of the interactions between the dust particle and the electric field. This is important for understanding the behavior of dust particles in the system, and for predicting the performance of the system. From the background theory it is noticed that there are different forces and phenomena acting on a particle when using an electrodynamic screen. Those of importance are the following:

- F_g Gravitational force (Equation 3.4)
- F_d Air drag force (Equation 3.5)
- F_C Coulomb forces (Equation 3.8)
- F_{sa} Surface adhesion (Equation 3.10)
- F_{DEP} Dielectrophoresis (DEP) force (Equation 3.12)
- F_g surface friction forces (Equation 3.14)

By utilising Newtons law of motion on the particle the forces acting on the particle can be written as:

$$m_p \frac{d}{dt} \vec{v} = \vec{F}_g + \vec{F}_d + \vec{F}_C + \vec{F}_{sa} + \vec{F}_{DEP} \quad (5.7)$$

Where m_p is the mass of the dust particle and \vec{v} is the velocity vector of the particle. Some of these forces may itself be functions of position, velocity or accelerations. Which makes the problem difficult. Nerveless Some estimations can be done.

5.8.1. Particle repulsion

At a certain point the particle will be repelled by the applied electric field. This happens when the repelling force is greater than the adhesion and gravity forces. This happens when the following relationship has to be satisfied:

$$F_{e_y} > F_g + F_{co} \quad (5.8)$$

by filling in Equation 5.8 with Equations 3.11, 3.4 and 3.8 the following equation for separation from the surface can be derived: This equation is also derived in [28]. We assume that the dust removal driving force generated on the particle is primarily due to the coulomb force.

$$|E_y| \geq \sqrt{\frac{4}{3\epsilon_0} \pi r_d^2 \rho G_s + \frac{c \cdot s^2}{\pi \cdot r_d \cdot \epsilon_0}} \quad (5.9)$$

The minimum electric field of repulsion depends on the radius r_d of the particle it can be evaluated for different values of the radius of the particles. This results in Figure 5.8. The situation on the Moon (blue) and on Earth (red) is plotted.

Its important to see that the adhesion forces become dominant when the particle becomes smaller. This can be seen in Figure 5.8 where particles of one micron will require a high electric field potential to be rejected from the surface.

We have determined which particles may end up on the surface of the solar panel. This is summarized in Table 3.2. If we take a closer look at Figure 5.8, the gravity forces are not dominant in the diameter range of 0 – 100 μm . Because the gravity of the moon lines up with that earth seen in Figure 5.8.

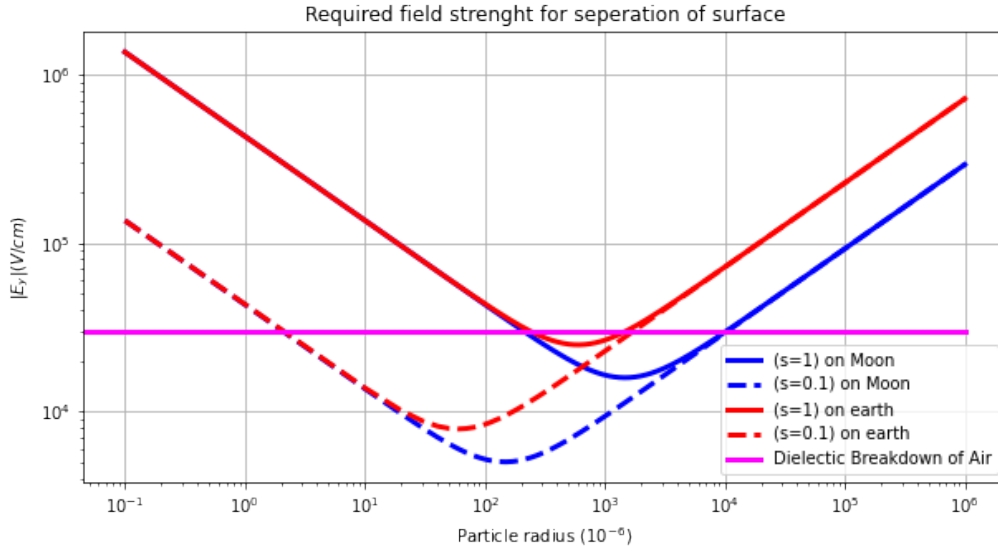


Figure 5.8: Minimum electric field for particle to escape, for Moon and Earth gravity with different surface cleanliness factors. Assuming Coulomb forces are dominant and neglecting air drag. Pink gives the dielectric breakdown of air.

5.8.2. Neglecting gravity on Field strength

Due to the specified particle size, gravity forces can be neglected in the modeling equation. Furthermore, the Lunar Zebro rover can tilt its solar panel almost horizontally (Section 3.1), which also reduces gravity forces with a term $\cos(\phi)$, where ϕ is the angle of the solar panel. See the full equation in A.52. Due to this effect, the electric field strength equation can be reduced to.

$$|E_y| \geq \sqrt{\frac{c \cdot s^2}{\pi \cdot r_d \cdot \epsilon_0}} (V/m) \quad (5.10)$$

equation 5.10 will be further used.

Because this project focuses on the particle size of $0-100\mu m$. We assume that the particles will remain on the surface primarily when the solar panel is tilted. This is also supported by the fact that gravity on the moon is around 3 times less than that on Earth.

5.8.3. Determining Electric field required for dust removal on the moon

The first thing that we can equate is the minimum electric field required for removal. This is described by Equation 3.11. With the particle described in Table 3.2, by filling a typical surface cleanliness of 0.88 from Section 3.5.4, the minimum electric field needed for the design. The particle range size of $1-100\mu m$ is taken:

Electric Field Strength in the y Direction
$3.2 \cdot 10^6 < E_y < 3.2 \cdot 10^7 (V m^{-1})$

The question is: are these values realistic? Is it necessary for a system to require a field strength of $32MV$? The answer is no, because smaller dust particles have less of an influence on the efficiency loss. Because they are smaller in size and thus conduct light better (Section 3.3.1)

From the experiment, it has been observed that relatively smaller particles stick more to the surface than larger particles, as can be seen in Figure C.4. This means that the required field strength has not been reached for removing these small particles.

5.9. Modeling switching frequency

After estimating the strength of the electrical field, other quantities can be estimated, namely the switching frequency of the electrodes. The proposed approach is as follows.

Again starting with a force model that consists in this analysis of the Coulomb forces F_c , drag force F_d , on the particle, the following equation is constructed.

$$F_{particle}^{\vec{}} = \vec{F}_c + \vec{F}_d \quad (5.11)$$

We will simplify the model to only the Coulomb force. Because there is no atmosphere on the moon which is able to generate drag forces on the particles. Equation becomes:

$$\overline{x''}(t)m = Q \cdot \vec{E}(x) \quad (5.12)$$

This is a second-order differential equation. Because the field strength $\vec{E}(x)$ depends on position.

Its assumed that a particle has to travel on average a length of $l = p + w$ This is the pitch between the electrodes and the width of the electrode. The switching frequency is defined as followed:

$$f_{min} = \frac{1}{t_{travel}} = \frac{1}{\frac{l_{electrode}}{v_{electrode}}} = \frac{v_{electrode}}{l_{electrode}} \quad (5.13)$$

If we simplify this problem, and make an assumption about the electric field $\vec{E}(x)$ to be uniform which makes it independent of the position x . Using equations 5.12 and 5.13. The following equation can be constructed for frequency.

$$f_{min} = \frac{1}{\sqrt{\frac{(w+p) \cdot 2m}{Q \cdot |E|}}} \quad (5.14)$$

If we have a charge density defined by $\rho_Q = \frac{Q}{m}$, the equation 5.14 becomes independent of mass. So the equation becomes:

$$f_{min} = \frac{1}{\sqrt{\frac{(w+p) \cdot 2}{\rho_Q \cdot |E|}}} \quad (5.15)$$

5.9.1. Determining Switching frequency

By filling in the values defined for a general moon dust particle described in Section 3.7. The switching frequency is expected to be below 100Hz . The following Figure (5.9) shows the switching frequency depending on the width plus pitch since this is the distance to travel. This is done for a typical particle charge a charge of $0.02 \cdot 10^{-3}$ Coulomb due to the tribocharging effect.

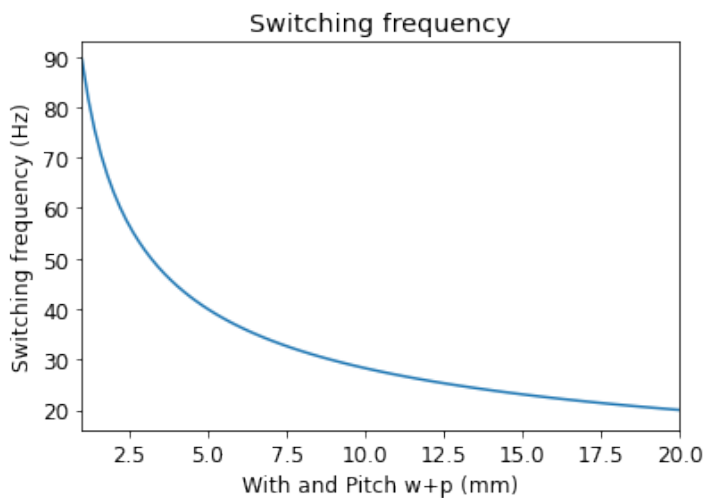


Figure 5.9: Switching frequency as function of width plus pitch of a particle with charge of $0.02 \cdot 10^{-3}$ Coulomb and electric field strength of $|E| = 8 \cdot 10^5$

H. Kawamoto et al. [40] did research on the dependence of frequency on the traveling particle. From his findings, higher frequencies increase the transportation of particles. But This does not mean the cleaning efficiency because of back traveling particles. As a side note the testing of EMI EMC requirements has been omitted, primarily based on a thorough review of the literature and considering the **low energy** and **frequency** of the electromagnetic field. Given these factors, it is anticipated that no show stoppers will arise from these constraints.

Experimental Evaluation

Using the architecture types from the literature and the available parameters following from the EDS model, a selection of designs was constructed for a first testing round. The goal of the first iteration was to show that the concept of removal is possible and to get an insight into the performance of the different architectures found in the literature. The mutual capacitances found also supplies the driver group with the information necessary for their design. For cheap and straightforward production of the EDS, it was decided to design PCBs in which the traces are used as the electrodes. For automatic generation of these PCBs scripts which could take design parameters as input were created. These can be found in Appendix B.2. For the second iteration the parameters of the zigzag architecture, which was shown to obtain the best performance during iteration one, were further explored.

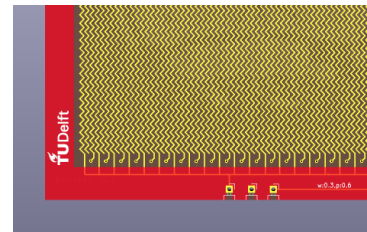


Figure 6.1: A render of one of the PCB designs

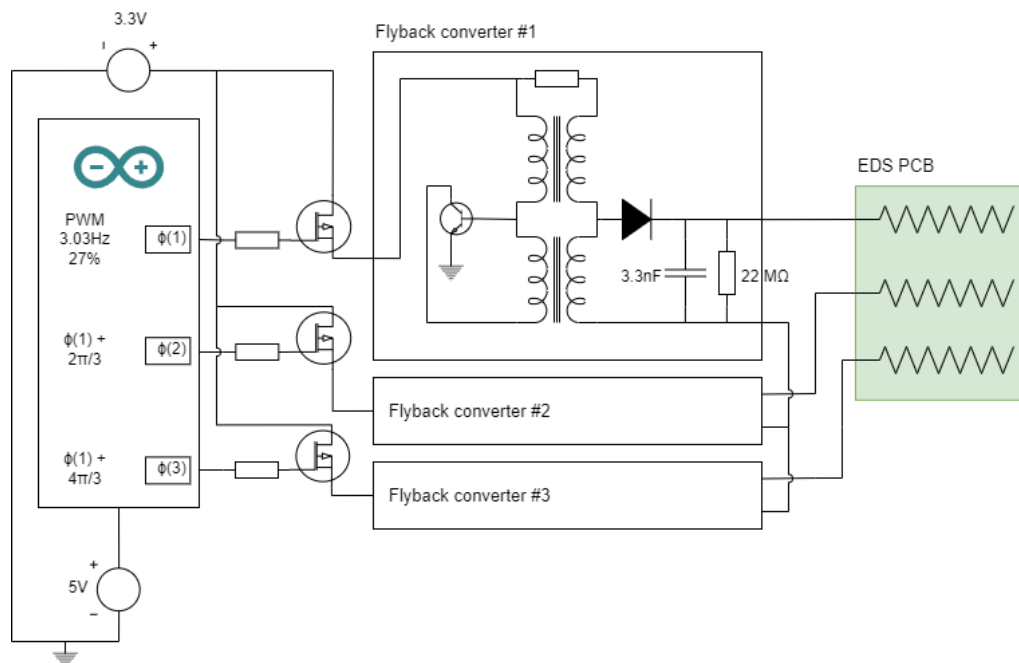


Figure 6.2: Schematic of the system.

6.1. Experimental setup

Since the project group that creates the system that drives the electrodes started at the same time, no circuit was available for testing purposes. Therefore, an off-the-shelf flyback converter was used to drive each electrode phase. These flyback converters were driven by an Arduino and MOSFETs. Figure 6.2 contains a schematic of the system. The RC time that follows from the capacitor and resistor at the output of the flyback converters limits the maximum frequency of the system. The same capacitor is also responsible for the safety of the system. For $R = 22M\Omega$, $C = 3.3nF$, $V = 1600V$ this system stays far under the lethal range:

$$\tau = RC = 0.073s, E = CV^2/2 = 0.0042J \quad (6.1)$$

To measure the high voltages on the electrodes, a straightforward approach involves utilizing a large Ohmic resistance in conjunction with a micro-amp meter to measure the current. By applying Ohm's law, the voltage can be calculated. The large resistance is necessary to prevent drawing an excessive current from the flyback converter, as this results in a drop in the supply voltage output due to loading. For both rounds of experiments, similar equipment is used. The difference between the experiments, aside from the different EDS designs, is that for the second the simulant [12] is used instead of the sieved sand. Weighing was performed with a scale with a precision of 0.01 gram. During testing, this turned out to be not precise enough. Therefore, for the first iteration, it was decided to slowly add a measurable amount of material over a fixed period of time.

6.2. Iteration 1 - Proof of concept

The first set of designs aimed to achieve several objectives. These are as follows:

- Provide a proof of concept to demonstrate the feasibility of the EDS system.
- Observe and analyze variations in dust removal mechanisms among the different designs. This allowed for a better understanding of how each design affected the removal of dust particles from the screen
- Measuring the mutual capacitance for comparison with the model
- Confirm the correct assembly of scripted PCB production.

6.2.1. Design

The initial designs, serving as a proof of concept, utilized different electrode architectures from the literature. Since it was not clear beforehand at what voltage the system could and would be tested, designs with different pitches were constructed. The details of these designs can be found in Table 6.1, while renders of the entire geometry can be found in Appendix B.1.2

Table 6.1: Different designs and their parameters

Design Number	Electrode pattern	Width	Pitch
1	Parallel	0.3 mm	0.6 mm
2	Parallel	0.3 mm	0.9 mm
3	Zigzag	0.3 mm	0.6 mm
4	Spiral	0.3 mm	0.5 mm
5	Spiral	0.13 mm	0.3 mm
6	2 phase zigzag & parallel	0.3 mm	0.6 mm - 0.13 mm

6.2.2. Test procedure

To compare the three different architectures, the EDS PCBs were loaded with 0.5 g of dust over a period of three minutes. This way the impact of clumping of particles could be reduced, so that a performance difference between designs can be measured. An overview of the test setup can be seen in Appendix C.1. A Pulse Width Modulation (PWM) signal with a duty cycle of 27% and a frequency of 3.03Hz was selected for the tests. For the traveling wave, three shifted copies of this signal with an amplitude of

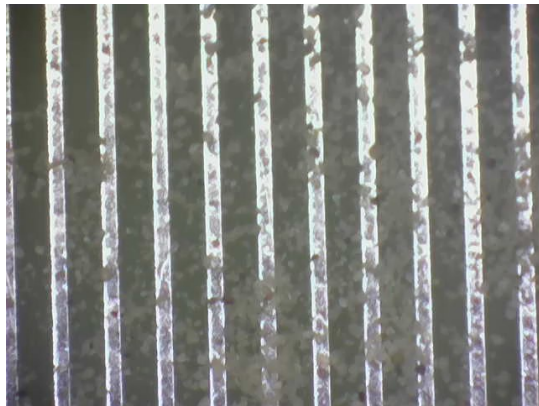
1600V were created. After the three minutes, the remainder was weighed. The exact test plan can be found in Appendix C.1.

6.2.3. Results

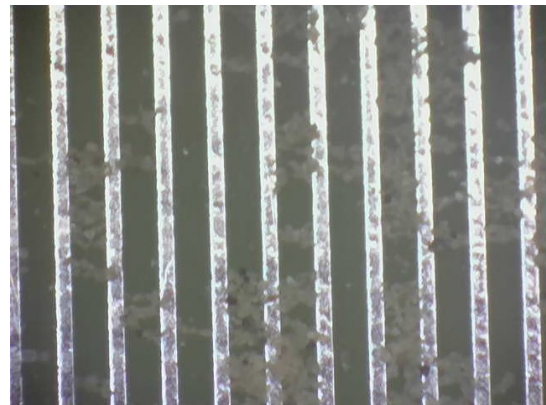
In Figure 6.4, it can be seen that after the system has been turned on, there are fewer particles present on the screen than before. Where particles are still present, they primarily exist in clumps. This clumping, that can be seen in Figure 6.3 played a large role in test results, as when turning the EDS on after a quantity of for example 0.50g is deposited, the removal efficiency is not measurable. When material is slowly added, the results do show a difference between the different architectures. In Table 6.2 these results can be seen, and the zigzag design clearly performs better than both the parallel and spiral design. This validates the findings of [36]. An explanation for this is the effect of field enhancement, as described in Section 3.4.3. In Figure 6.5 the field strength is simulated for a 1kV potential between two electrodes for both the parallel and zigzag architectures, and the enhancement can be clearly seen. This results in the electric field having a larger vertical electrical field between the electrodes, which was simulated in Figure 6.6. The geometry and settings used for these simulations can be found in C.4. The frequency was also varied within the possibilities of the test system. No change was seen in what particles could be removed, only in the speed with which they moved. The mutual capacitance values ranged from 100 pF for the parallel electrode design with the largest pitch to 250pF for the spiral design with the smallest pitch. All values can be found in Appendix C.2. The values calculated with the formulas from Appendix A.6.3 can also be found there. For a voltage below 4,5kV and a frequency below 50Hz, the power usage of a 250pF EDS system is below 0.125W.



Figure 6.3: An example of clumping



(a) Initial Surface covered



(b) After 4.50 seconds when the dust removal system is turned on. Mostly what is still left are clumps of particles.

Figure 6.4: Comparison of surface conditions

The following conclusions can be drawn from the first test and are the basis of the second iteration.

- The zigzag structure clearly demonstrated higher efficacy in removing dust compared to both the parallel electrodes and the spiral design.
- Breakdown phenomena were observed in the vicinity of sharp corners for the smallest pitch sizes. Although this is a very effective way to remove dust (Figure 6.7), this is not energy efficient or good for the longevity of the system. In the lunar atmosphere this only becomes an issue when breakdown occurs between the dielectric. This requires a much higher voltage, as can be read in Section 3.4

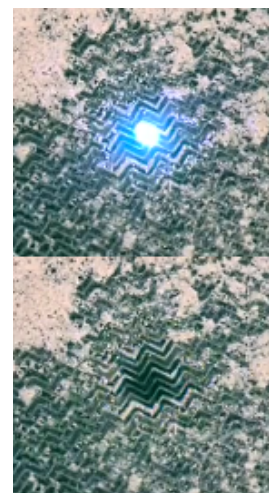


Figure 6.7: Dust removal by breakdown

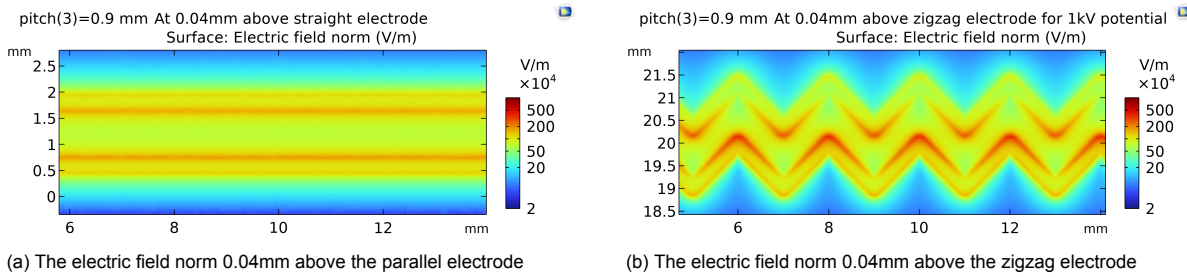


Figure 6.5: Top-down comparison of the Electrical field to show the field enhancement of the zigzag architecture

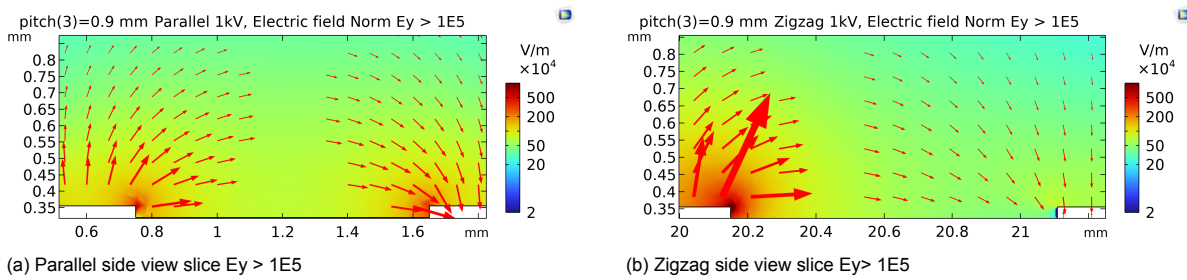


Figure 6.6: Side view comparison of the Electrical field with vector arrows filtered for $|E_y| > 1E5$. It can be seen that the parallel architecture has a larger gap of vector arrows between the electrodes.

- Based on visual observations, it was noticed that particles that clump together between electrodes are challenging to remove compared to individual particles.
- Dust particles tend to accumulate in the central region between the electrodes. This can be attributed to the electric field in the y-direction being insufficient for removal in those areas. Consequently, there is no counter force against the gravitational and cohesive forces acting on the particles, leading to their aggregation in that region. This finding was the basis for driving a design equation about the minimum requirements for E_y .

After conducting tests, the zigzag design has been selected for further study and enhancement. However, there is still a clear issue regarding dust accumulation between electrodes or in areas where the intensity of the electric field (E_y) is not sufficient. The outcome of the COMSOL simulation provides an explanation of the electrode behavior, but monitoring the behavior of individual particles proves challenging due to its unpredictable nature. Another takeaway is that the traces on the PCB are extruded a bit above the dielectric, which might hinder particle removal. This effect can be reduced by adding a solder mask.

Table 6.2: Measurement results travelling wave EDS

	Before (g)	After (g)
Parallel (D1)	0.54	0.21
Zigzag (D3)	0.49	0.11
Spiral (D4)	0.51	0.36

6.3. Iteration 2 - Zigzag parameter variation

The purpose of the second design iteration was to further study the effect of field enhancement in the zigzag design. Six designs were made, which are a combination of two angles for three different pitches. The exact design parameters can be seen in Table 6.3. Another goal of the experiment was to see if the usage of LHS-1 Moon simulant instead of sand would result in any effects not seen before.

6.3.1. Design

Table 6.3: Design parameters second design iteration

Design number	Unit Length [mm]	Angle [degrees]	Width [mm]	Pitch [mm]
D1	1	90	0.13	0.12
D2	1	90	0.13	0.3
D3	1	90	0.13	0.6
D4	2	130	0.13	0.12
D5	2	130	0.13	0.3
D6	2	130	0.13	0.6

6.3.2. Visual findings

The information obtained from the scale setup was less informative compared to the previous experiment, as the performance difference is no longer large enough to be measurable by the scale used. For a deposition of 0.50g of dust, clumping still plays a large role in the effectiveness of removal. For smaller amounts of dust, the clumping can sometimes be overcome, as can be seen in Figure 6.8.

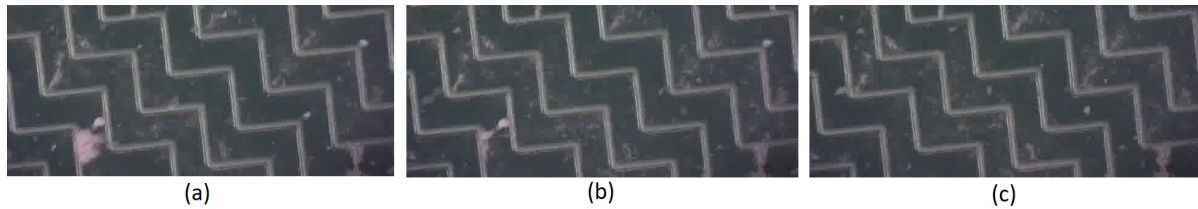


Figure 6.8: The removal of clumped particles (bottom left) for a 90 degree zigzag design over the span of a second.

By comparing the electric field simulation with the test results as seen in Figure 6.9, it can be inferred that dust accumulation still occurs in regions where the electric field strength is insufficient. However, it is noticeable that sharper corners in the design lead to stronger electric fields, resulting in reduced dust accumulation. When comparing the tests with the results when using sand, a notable change is the smaller impact that clumping seems to have. This could be explained by the lower humidity of the material, which results in lower Van der Waals forces. In Figure 6.10 another difference can be seen. A number of small particles gathered primarily in the regions mentioned above. These particles are so small that the Coulomb force is not sufficient to overcome the relatively larger adhesion force, as was hypothesized in Figure 5.8.

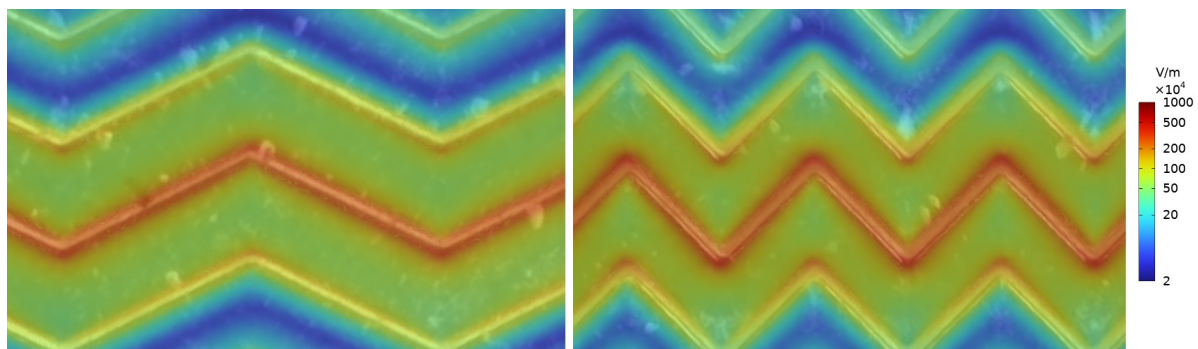


Figure 6.9: COMSOL Simulations at 0.04mm above the electrodes where the middle electrode was supplied with 1kV overlaid on visual of experiment



Figure 6.10: Small particles not removed

Integration and efficiency

For the Lunar Zebro mission it is important to characterize the efficiency loss due to the additional layer of material on the solar panel. For testing purposes, copper electrodes are used. These electrodes are not transparent and block all the light. It's assumed that transparent electrodes behave similarly when used for electrodes of a EDS system to that of the copper ones.

7.1. Transparent ITO

Indium tin oxide electrodes (ITO) are thin films of indium tin oxide used in a variety of applications, such as touchscreens, solar cells, and organic light-emitting diodes (OLEDs). ITO electrodes are typically made by sputtering a thin layer of indium tin oxide onto a substrate, such as glass or plastic. The resulting electrode is then patterned to create the desired shape and size. ITO electrodes are widely used in the electronics industry because of their excellent electrical and optical properties.

However, these electrodes are not completely transparent and will have an effect on the transmission of light. The problem becomes more difficult because the absorption of this material depends on the wavelength of light. For example, a $2\mu\text{m}$ film of tin oxide will have an effect on the solar radiance. This is visually shown in Figure 7.1.

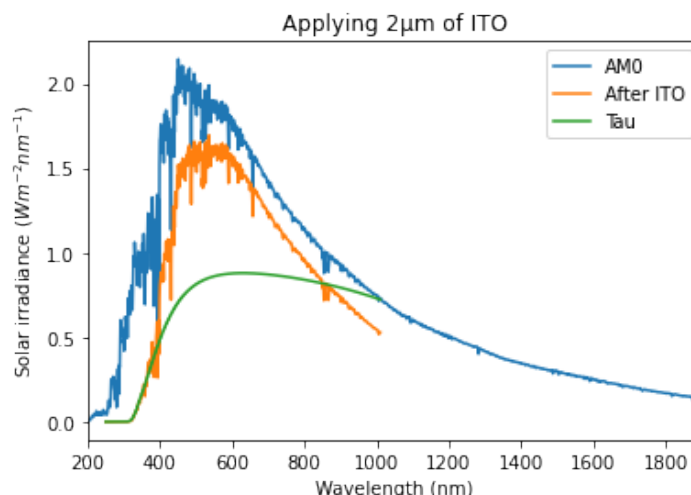


Figure 7.1: Air mass 0 spectrum after transmission through $2\mu\text{m}$ of indium tin oxide. Where Tau is the transmission coefficient

After an indium-tin oxide layer is deposited on the solar panel, light absorption is not uniform. The absorption is most noticeable in the wavelength region of 300 and 600 nm. This can also be observed in Figure 7.1

For construction of this figure, refer to Appendix A.8

7.2. Solar panel efficiency

Because ITO influences blue light and the solar panel is a triple junction solar cell. One of the junctions may limit the solar cell current generation, The electrical circuit is schematically drawn in Figure C.6.

The power generated by a triple junction solar panel is approximated by the following equation.

$$P_{ITO} = \min(|I_{sc1}|, |I_{sc2}|, |I_{sc3}|) \cdot (V_{oc1} + V_{oc2} + V_{oc3}) \cdot FF \quad (7.1)$$

Where FF is the fill factor which is typically taken to be 0.88. I_{scn} is the short circuit current in amps (A) through each solar cell which is given by Equation A.37. V_{oc} is the open circuit voltage in volt (V) which is given by Equation A.43.

The efficiency loss can be expressed by the following equation:

$$\eta_{ITO} = \frac{P_{ITO}}{P_{Without-ITO}} \quad (7.2)$$

By evaluating Equations 7.1 and 7.2. With taking the quantum efficiency's, AMO and transmission coefficient. The following Figure 7.2 can be constructed for the efficiency decrease of the solar panel due to a layer of ITO.

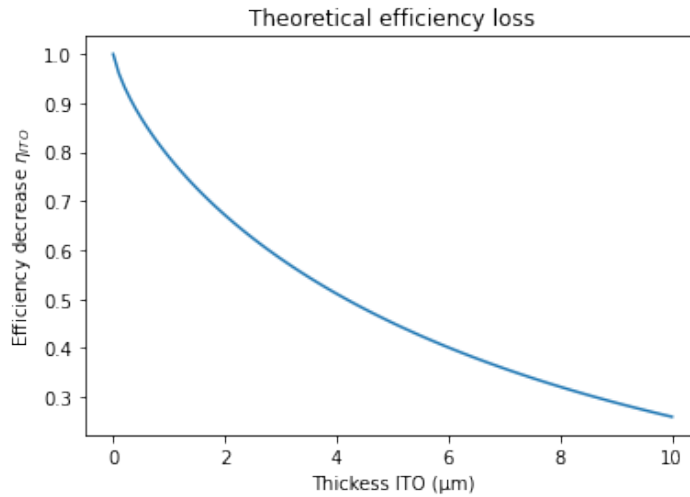


Figure 7.2: Relative Efficiency loss due to ITO

For a layer of $0.1\mu m$, the efficiency of the solar panel is 92%. Therefore, we have an efficiency reduction of 8%. Using a layer of $1\mu m$ will reduce the efficiency of the solar panel to 76% of its initial production. This calculation is for a fully covered panel with ITO. Therefore it's important to have a weight factor in relation to the coverage of the panel. This is defined as the coverage factor η_{cover} :

$$\eta_{cover} = \frac{w}{w + p} \quad (7.3)$$

Here w is the width and p is the pitch of the electrode. The coverage factor plays a crucial role in assessing the effectiveness of the EDS system. Increasing the coverage area may result in a decrease in efficiency. Therefore, it is important to find the optimal balance between the required electrode area and the generated electric field.

When taking a coverage of 50% and placing a layer of $0.1\mu m$ of ITO on top of the solar panel the theoretical solar radiance is reduced to only 4%. The same for $1\mu m$ the theoretical efficiency decrease is estimated to be 12%.

7.3. Dust deposition on panel

It's important to quantify the dust deposition on the rover. When taking 4000 particles per day from Section 3.3.1. The equivalent mass deposition on the panel is evaluated by filling in Equation A.1.

Taking the particle radius to be around $50\mu\text{m}$, $\rho = 2750\text{kg m}^{-2}$ This results in a particle deposition of around $720\mu\text{g m}^{-2}$ per day. The area of the solar panel is around 365cm^2 Thus the deposition on the solar panel of Lunar Zebro becomes around $26\mu\text{g}$ per lunar day.

Using Equation 7.1 again, by interpolating the solar spectrum AM0 seen in Figure 7.1 with Equations 3.3.1. The following figure is constructed.

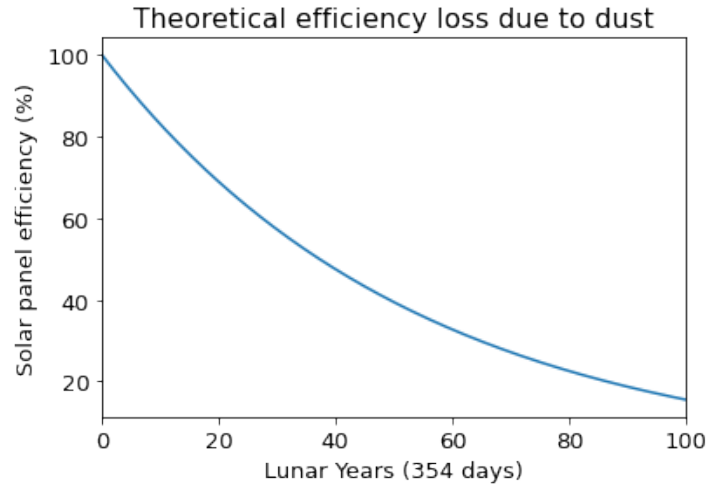


Figure 7.3: Estimated solar panel efficiency for the Rover of Lunar Zebro[6] based on data of collected from LEAM [17] This is for uniform coverage of dust.

What is noticeable in Figure 7.3 is that dust deposition when assuming 4000 particles per day per square meter. That it is rather slow. The solar panel efficiency decrease looks like a multi-year process.

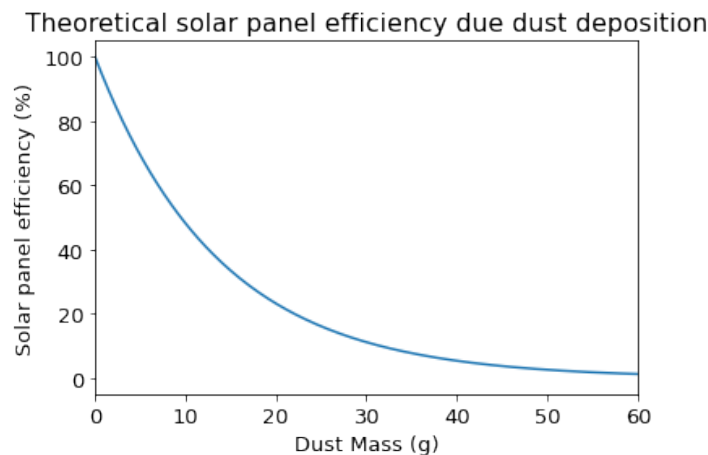
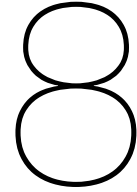


Figure 7.4: Solar panel efficiency due to dust mass on solar panel

The theoretical calculation of the impact of mono layer dust deposition on efficiency is consistent with the findings of the experimental research in [19]. The Figure of A.4 and Figure 7.4 show the exponential loss of efficiency and power caused by the accumulation of dust. Based on the time and expected quantity of lunar dust to be deposited, this conclusion can be used to determine the necessity of EDS.



Feasibility and the proposed design

”Is Lunar Dust a Problem for the Lunar Zebro Moon Rover’s mission?” The amount of dust that will accumulate on the solar panels is unknown but it is directly related to the mission’s duration. In case of the mission duration of 14 days the effect of dust particles on the efficiency of solar panels are marginal. However for longer mission duration or in case of dust generation due the reasons discussed in the background study the efficiency of solar panel will be decreased to a problematic state. In that case a dust mitigation strategy is necessary.

The second part of the main question namely **”how may these impacts be minimized to prevent problems with energy harvesting?”** was concerning minimizing the effect of dust on the solar panels. Based on the information and testing given thus far it is possible to employ the EDS system in the event that dust were to accumulate. Such a design could be reasonable if the efficiency of solar panel would drop more than 97 percent due to presence of the dust particle. The solar panels’ effectiveness with a careful design which will provided shortly would not be hampered by the electrode covered area, and the dust would be effectively eliminated and the efficiency of solar panels will be restored. In this chapter, the specifics of such a design will be covered.

8.1. Proposed Design

8.1.1. Setting the parameters

Various designs were examined throughout the course of this project, and due to field enhancement by sharp corners, the zigzag architecture performed better than the other possibilities. As a result, the electrode architecture was decided to be zigzag.

The goal of such a design is to have the transmission coefficient T as high as possible, Coverage factor η_{cover} as small as possible to avoid decrease of absorption of irradiance and E_y should be maximised for particles to be repelled. Because of its electrical properties and transparency, ITO is a good contender for electrode material. To achieve this the electrode width choice has to be lower than $1 \mu m$ so that it would have low impact on the efficiency of the solar panel. The choice of pitch has less constrains. The closer the electrodes are (hence the lower the pitch), the greater the electric field and the smaller area with E_y that does not match the minimal criterion. However, there may be other constraints on the pitch, such as material breakdown, and temperature restrictions. The width and pitch parameters for this recommended design are 1 mm and 1 mm, respectively, however these can be altered for a customized design. The operating voltage of such a proposed EDS design is ideally as high as feasible while preventing material breakdown. However, to prevent issue with the electronic team’s requirements for available MOSFETs max voltages and also non lethality of the system voltages lower than 4.5 kV are advised. The frequency has effect on the speed of dust removal. The impact of frequency on the efficiency of dust removal is to be determined but from the preliminary analysis is not the dominant factor. From analysis switching frequency’s below 100 Hz is determent. Lower frequency is recommended to minimise the amount of energy loss per cycle. Due to the charging and discharging of the electrodes. Also for space missions of Zebro, The time scale of the cleaning cycle is in the order of minutes.

8.1.2. Modes of operation

Aside from clever design decisions for choosing the parameters, the control and operating modes of the EDS system are critical. Through the tests it was observed that the dust particles that are clumped together are more difficult to remove and therefore this situation should be prevented. The system operates effectively when the EDS system is turned on while the particles are depositing on the solar panel, according to visual tests. As a result, it is recommended to utilize an EDS system where it is believed that the rover will operate in regions with a high probability of dust deposition, such as in the proximity of other lunches, lunar rovers, and other sources that might cause dust circulation. Aside from that, a periodic operation is recommended to avoid dust particles from clumping, which makes removal more difficult. The period is determined by the rover's energy budget and mission duration which are to be developed at this stage. During this time, the rover can execute the so-called **cleaning cycle**, which consists of rotating the solar panels to be horizontal to decrease the influence of gravity and cohesive forces. Then, by activating the EDS system, the likelihood and efficiency of particle removal increases. The duration of such a cycle does not need to be extensive, and as demonstrated in the test, dust removal appears to saturate within a few minutes. As a result, 5 minutes is more than enough time to maximize the effectiveness of each cycle. Through control analysis, it is feasible to maximize energy capture. This is required for TRL 5 and above cases to ensure maximum energy gain and a more accurate answer for the number and duration of cleaning cycles. A through control analysis has been proposed by [53] for EDS systems.

8.2. Recommendations regarding testing

The test have been performed in the course of this project are mainly intended for TRL 3 and possible 4 stage, however the test configuration did not adequately represent the environment in which the system should work. The purpose of this section is to describe a configuration that will allow for outcomes equivalent to a system on the moon.

1. **Vacuum** The presence of air has a big impact on the experiments. In section 4.3 it was found that the humidity of air has a negative effect on removal efficiency. The particle trajectories are also impacted by drag. The system voltage can also be limited by the low breakdown strength of air. Its important to keep in mind Paschen's law given in section 3.4. Due to the reduction in breakdown voltage when gas pressures are decreased.
2. **High precision digital scale** In [15], the relative power output of a solar power covered by just $2mg/cm^2$ of Mars simulant is 65%. Since small quantities of dust have a large impact, it is necessary to take precise measurement.
3. **Lunar Simulant** As was seen in section 4.3, the simulant is a conservative way to test for actual lunar dust. This material should be dried beforehand for an accurate comparison.
4. **Lab requirements** It is important to keep in mind that silica dust, which the simulant is mostly composed of, is classified as a human carcinogen[54]. The particles should therefore not be inhaled. A good practice that was used for the tests with simulant in this report is to first do a dry-run with sieved sand. Another safety remark is that even though the energy requirements of the system are low, the voltage is high.
5. **Optional: High speed camera** To support claims about the mechanism behind the removal, it could be very helpful to have a good insight of the path the particles take. In such cased the theoretical calculated particle trajectories can be evaluated which would give insight about the behaviour of EDS systems.
6. **Optional: Adjusted Gravity** In Section 5.8.2 it was found that gravity can be neglected for the relevant particle size the impact of gravity on the minimum vertical field strength for removal. This combined with the complexity of generating this reduction results in this not being a recommended part of the final test setup.

9

Conclusion

During the project, an EDS screen was constructed that was capable of removing dust from a 100 x 100 mm area without containing moving parts utilizing the electric field generated by a large potential between the electrodes. An overview was given of how and why certain parameters impact the effectiveness, energy usage, safety, and transparency of such a system. The zigzag architecture was experimentally found to be the best performing. The measured capacitance of the EDS system, in combination with a maximum voltage of 4.5kV, results in a system that is nonfatal when accidentally touched. For the maximum suggested frequency of 50Hz, these same parameters result in a system that consumes maximally 1/8th of the required power usage limit. This relatively low operating frequency of the EDS system, compared to the communications operating frequency, results in a negligible amount of EMI.

When the electrodes of the EDS are theoretically constructed with ITO, the loss for a coverage of 50% it can be as low as 4% for a thickness of $0.1\mu\text{m}$ and for $1\mu\text{m}$ the theoretical efficiency loss is estimated to be 12%.

Even though this loss is very little, based on the limited information available that we have, implementing this system is not recommended for a mission duration of 14 days. The impact the natural deposition has on the solar performance is too little to justify such a system. If there are either other sources of deposition, or if the amount of particles naturally deposited is revalued this decision should be reviewed. The system may not remove really fine particles starting $< 1\mu\text{m}$ particle decomposition onto the surface. This is due to the higher field strengths needed. This is concluded from Section 5.8.1 and also visually observed.

9.1. Discussion

Something that plays a large role in determining the utilization of such a system, is the amount of dust that ends up on the rover. Only one source has been found, from an experiment that was not set up for gathering that data. If based on research that does not yet exist or that is not publicly available this deposition rate is reevaluated, this recommendation could change drastically. Another reason for integrating the EDS system would be the deposition of dust by mission activity. This can range from the rover kicking up dust itself to nearby landings or launches.

The exact properties are another point that is open for discussion, especially when other sources of deposit are considered. If the rover kicks up the dust itself, which might be particles larger than $100\mu\text{m}$, the dominant forces for determining the required field changes from adhesion forces to gravity. By changing the orientation of the solar panel this dust may fall off of the panel itself.

The information about the particles being lofted is based on models. It might be the case that the average particle size lofted is much smaller than that the mean size of the simulant. This would be an issue, since it was shown that these smaller particles can be harder to remove.

9.2. Future research

In this report all tested designs are standard PCBs which lack transparency. The effect ITO electrodes have on the efficiency of the solar panel has been worked out theoretically, but problems might arise when actually implementing this material. This should be tested further. The testing should be performed in a way that accurately represents the situation on the Moon. For this the guidelines are given in Chapter 8. The EDS system works with strong electric fields. These strong fields might in some way impact the workings of the solar panel, especially when the distance between interconnects and electrodes is very small for transparency reasons.

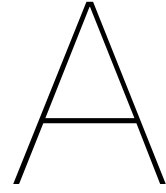
Bibliography

- [1] Z. M. Dlugach, O. I. Korablev, A. V. Morozhenko, V. I. Moroz, E. V. Petrova, and A. V. Rodin, "Physical properties of dust in the martian atmosphere: Analysis of contradictions and possible ways of their resolution," *solar system research*, vol. 37, pp. 1–19, 2003. [Online]. Available: <https://doi.org/10.1023/a:1022395404115>
- [2] R. Sharma, C. Wyatt, J. Zhang, M. K. Mazumder, C. I. Calle, and N. Mardesich, "Performance analysis of electrodynamic self-cleaning transparent films for its applications to mars and lunar missions," in *2007 ieee industry applications annual meeting*, 2007, pp. 434–437.
- [3] S. Masuda, K. Fujibayashi, K. Ishida, and H. Inaba, "Confinement and transportation of charged aerosol clouds via electric curtain," *electrical engineering in japan*, vol. 92, pp. 43–52, 1972. [Online]. Available: <https://doi.org/10.1002/eej.4390920106>
- [4] A. V. Zakharov, L. M. Zelenyi, and S. I. Popel', "Lunar dust: Properties and potential hazards," *solar system research*, vol. 54, pp. 455–476, 2020. [Online]. Available: <https://doi.org/10.1134/s0038094620060076>
- [5] M. Abbas, D. Tankosic, P. Craven, J. Spann, A. LeClair, and E. West, "Lunar dust charging by photoelectric emissions," *planetary and space science*, vol. 55, pp. 953–965, 2007. [Online]. Available: <https://www.sciencedirect.com/science/article/pii/S003206330600359x>
- [6] M. K. Verma, P. Sachdeva, C. Verhoeven, A. Menicucci, R. T. Rajan, and A. Noroozi, "Lunar zebro - nano rover tu delft."
- [7] J. Bacani, "Lunar rover solar panel deployment system."
- [8] AzurSpace, "Tj solar cell assembly 3g30a."
- [9] O. Isabella, K. Jäger, A. Smets, R. van Swaaij, and M. Zeman, "Solar energy," 2016.
- [10] A. Shanbhag, "Redmoon: Radiation environment and dose monitoring on-board a nano-rover," 2022.
- [11] G. H. Heiken, D. T. Vaniman, and B. M. French, "Lunar sourcebook, a user's guide to the moon," 1991.
- [12] E. Lab, *Lunar Dust Simulant LHS-1 Fact Sheet*, 2022.
- [13] N. C. Orger, K. Toyoda, M. Cho, and J. R. Cordova Alarcon, "Lunar dust lofting due to surface electric field and charging within micro-cavities between dust grains above the terminator region," *advances in space research*, vol. 62, pp. 896–911, 2018. [Online]. Available: <https://www.sciencedirect.com/science/article/pii/S0273117718304411>
- [14] E. Grün, M. Horanyi, and Z. Sternovsky, "The lunar dust environment."
- [15] C. M. Katzan, D. I. Brinker, and R. Kress, "The effects of lunar dust accumulation on the performance of photovoltaic arrays."
- [16] NASA, "Lunar ejecta and meteorites - experiment." [Online]. Available: <https://nssdc.gsfc.nasa.gov/nmc/experiment/display.action?id=1972-096c-05>
- [17] J. E. Colwell, S. Batiste, M. Hor, aacute, nyi, S. Robertson, and S. Sture, "Lunar surface: Dust dynamics and regolith mechanics," 2007.
- [18] M. N. Horenstein, A. Sayyah, M. K. Mazumder, and R. S. Eriksen, "2performance analysis of electrodynamic screens based on residual particle size distribution."

- [19] J. Shahmoradi, A. Maxwell, S. Little, Q. Bradfield, S. Bakhtiyarov, P. Roghanchi, and M. Hassanaian, "Martian and lunar dust on solar panel," 2020.
- [20] F. Kreuger, *Industrial High Voltage: 1. Electric fields, 2. Dielectrics, 3. Constructions*. Delft University Press, 1991.
- [21] P. Atten, H. L. Pang, and J.-L. Reboud, "Study of dust removal by standing-wave electric curtain for application to solar cells on mars," *ieee transactions on industry applications*, vol. 45, pp. 75–86, 2009.
- [22] D. Faircloth, "Technological aspects: High voltage."
- [23] R. Latham, "High voltage vacuum insulation."
- [24] X. Wang, M. Horányi, C. Hartzell, and D. Scheeres, "Experimental demonstration of the role of cohesion in electrostatic dust lofting," *geophysical research letters*, vol. 40, pp. 1038–1042, 2013. [Online]. Available: <https://agupubs.onlinelibrary.wiley.com/doi/abs/10.1002/grl.50230>
- [25] C. Morales, "Modeling the particle transport."
- [26] J. Ping and Z. Meng, "Lunar surface electrical conductivity," pp. 1–3, 2017. [Online]. Available: https://doi.org/10.1007/978-3-319-05546-6_67-1
- [27] J. Schwan, X. Wang, H.-W. Hsu, E. Grün, and M. Horányi, "The charge state of electrostatically transported dust on regolith surfaces," *geophysical research letters*, vol. 44, p. 3059 – 3065, 2017. [Online]. Available: <https://www.scopus.com/inward/record.uri?eid=2-s2.0-85017555798&doi=10.1002%2f2017gl072909&partnerid=40&md5=f9ada588ee46cf856d48a61a8f598c53>
- [28] C. M. Hartzell and D. J. Scheeres, "The role of cohesive forces in particle launching on the moon and asteroids."
- [29] H. A. Perko, J. D. Nelson, and W. Z. Sadeh, "Surface cleanliness effect on lunar soil shear strength," *journal of geotechnical and geoenvironmental engineering*, vol. 127, 2001.
- [30] T. B. Jones, "electromechanics of particles," 1995.
- [31] L. H. Yeo, X. Wang, A. Dove, and M. Horányi, "Laboratory investigations of triboelectric charging of dust by rover wheels."
- [32] H. Kawamoto, K. Seki, and N. Kuromiya, "Mechanism of travelling-wave transport of particles," *journal of physics d: applied physics*, vol. 39, p. 1249, 2006.
- [33] R. Sims, A. Biris, J. Wilson, C. Yurteri, M. Mazumder, C. Calle, and C. Buhler, "Development of a transparent self-cleaning dust shield for solar panels," *proc. esa-ieee joint meeting electrostatics*, 2003.
- [34] R. Sharma, C. A. Wyatt, J. Zhang, C. I. Calle, N. Mardesich, and M. K. Mazumder, "Experimental evaluation and analysis of electrodynamic screen as dust mitigation technology for future mars missions," *ieee transactions on industry applications*, vol. 45, pp. 591–596, 2009.
- [35] S. J. Williams, J. D. Schneider, B. C. King, and N. G. Green, "particle-induced electrostatic repulsion within an electric curtain operating below the paschen limit," *micromachines*, vol. 13, 2022. [Online]. Available: <https://www.mdpi.com/2072-666x/13/2/288>
- [36] S. Saeidpour, B. Khoshnevisan, Z. Boroumand, and N. Ahmady, "Effect of electrode design and dust particle size on electrodynamic dust shield procedure."
- [37] H. Kawamoto, M. Uchiyama, B. Cooper, and D. McKay, "Mitigation of lunar dust on solar panels and optical elements utilizing electrostatic traveling-wave."
- [38] M. N. Horenstein, M. Mazumder, and R. C. S. Jr., "Predicting particle trajectories on an electrodynamic screen - theory and experiment."

- [39] Q. Sun, N. Yang, and X. Cai, "Mechanism of dust removal by a standing wave electric curtain," *science china physics, mechanics and astronomy*, vol. 55, 2012.
- [40] H. Kawamoto and N. Hasegawa, "Traveling wave transport of particles and particle size classification."
- [41] S. De, M. Kumar, S. Manna, S. Ghosh, K. Sinha, D. Adak, S. Maity, and R. Bhattacharyya, "Surface engineering of solar glass covers for soiling related issues by applying electrodynamic screens (eds)."
- [42] M. Mazumder, A. Biris, D. Saini, P. Srirama, R. Sims, C. Calle, and C. Buhler, "Electrodynamic removal of contaminant particles and its applications," vol. 2, pp. 1283–1286 vol.2, 2004.
- [43] Morales, Cristian, and Manuel, "Increasing dust removal efficiency of electrodynamic screens using frequency optimization via comsol multiphysics® c. morales, r. eriksen, m. n. horenstein, m. mazumder1 1. electrical and computer engineering, boston university, boston, ma, usaexcerpt from the proceedings of the 2017 comsol conference in boston."
- [44] Y. Yu, J. Cilliers, K. Hadler, S. Starr, and Y. Wang, "A review of particle transport and separation by electrostatic traveling wave methods."
- [45] T. Sarver, A. Al-Qaraghuli, and L. L. Kazmerski, "A comprehensive review of the impact of dust on the use of solar energy: History, investigations, results, literature, and mitigation approaches," *renewable and sustainable energy reviews*, vol. 22, pp. 698–733, 2013. [Online]. Available: <https://www.sciencedirect.com/science/article/pii/S136403211300021x>
- [46] M. N. Horenstein, A. Sayyah, D. R. Crowell, A. Raychowdhury, and M. K. Mazumder, "An experimental study on the characterization of electric charge in electrostatic dust removal," *journal of electrostatics*, vol. 87, pp. 173–179, 2017. [Online]. Available: <https://www.sciencedirect.com/science/article/pii/S0304388617300141>
- [47] U. R. Fawwaz T. Ulaby, "Fundamentals of applied electromagnetics 7th edition - fawwaz t. ulaby," 2010.
- [48] F. R. Zypman, "Mathematical expression for the capacitance of coplanar strips," 2019.
- [49] C. R. Harris *et al.*, "Array programming with numpy," 2020.
- [50] C. Multiphysics, "Introduction to comsol multiphysics®," *comsol multiphysics, burlington, ma, accessed feb*, vol. 9, p. 2018, 1998.
- [51] Python Software Foundation, "Python," 1991.
- [52] A. Meurer, C. P. Smith, M. Paprocki, and et al., "SymPy: Symbolic computing in python," *peerj computer science*, vol. 3, p. e103, 2017.
- [53] D. Qian, J. Marshall, and J. Frolik, "Control analysis for solar panel dust mitigation using an electric curtain," *renewable energy*, vol. 41, pp. 134–144, 2012. [Online]. Available: <https://www.sciencedirect.com/science/article/pii/S0960148111005799>
- [54] Exolith, "Safety data sheet lunar dust simulant," 2018.
- [55] E. C. Donaldson and W. Alam, "wettability," pp. 57–119, 2008. [Online]. Available: <https://www.sciencedirect.com/science/article/pii/B9781933762296500089>
- [56] H. C. Hamaker, "The london van der waals attraction between spherical particles."
- [57] J. D. Jackson, "Classical electrodynamics," 1962.
- [58] SciPy, *SciPy documentation — SciPy v1.11.1 Manual*. [Online]. Available: <https://docs.scipy.org/doc/scipy/index.html>
- [59] M. Polyanskiy, "Refractive index of in2o3-sno2 (indium tin oxide, ito) - konig," 2023. [Online]. Available: <https://refractiveindex.info/>

-
- [60] P. J. Verlinden, "Chapter ic-5 - high-efficiency back-contact silicon solar cells for one-sun and concentrator applications."
- [61] T. G. COMPANY, "Nema grade fr4 glass epoxy laminate," 2008. [Online]. Available: <https://thegundcompany.com/wp-content/uploads/2023/01/nema-fr4-from-the-gund-co.pdf>
- [62] R. F. Bautista, J.-P. Charras, and J. Evans, "Kicad pcbnew python scripting cheat sheet," 2015.



Appendix A

A.1. Mass of a particle

The mass of a particle is approximated with a spherical volume. The mass becomes:

$$m = \frac{4}{3} \cdot \pi \cdot r^3 \cdot \rho \quad (\text{A.1})$$

Where m is the mass in kg , r the radius of the particle in meters and ρ the density of the particle in kilogram per square meter ($kg\ m^{-2}$).

A.2. Hamaker constant

The Hamaker constant describes the interaction van der Waals energy (E_{vdw}) with the separation distance between two molecules. [55] [56]

$$A = \pi^2 C \rho_1 \rho_2, \quad (\text{A.2})$$

Where ρ_1 and ρ_2 are the number densities of the two particles and C is the London coefficient in the particle-particle pair interaction. The magnitude of this constant reflects the strength of the vdW-force between two particles. This can also be a substrate. [56].

A.3. Surface Cleanliness

The surface cleanliness is defined as [29]:

$$S = \Omega/t \quad (\text{A.3})$$

Where Ω is the diameter of an O^{-2} ion which is $1.32 \cdot 10^{-10}m$ and t is the adsorbate thickness. The value of S is bound between 0 and 1 with 1 being perfectly clean and zero being saturated soil. Its not intuitive if you look into equation 3.11 that the cohesion forces will decrease with surface cleanliet. But This is because clean surfaces have more atoms which can interact with the dust particles. A relative dirty surface with a lot of spikes have less molecules interacting with the particle this lowers the adhesion forces.

A.4. Experimental Efficiency results from papers

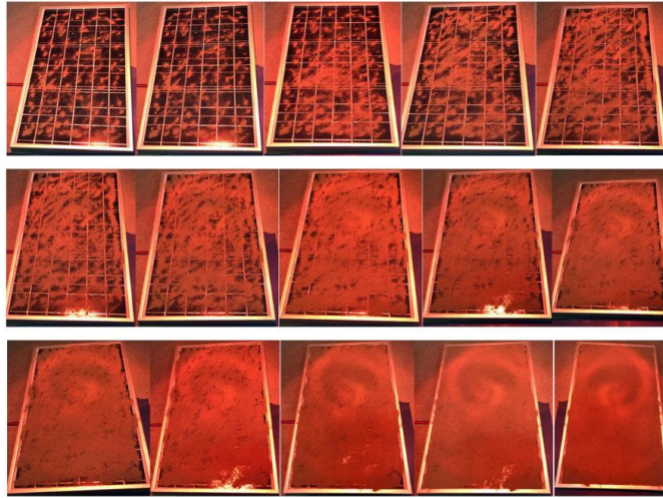


Figure A.1: Solar panels and dust deposition simulation [19]

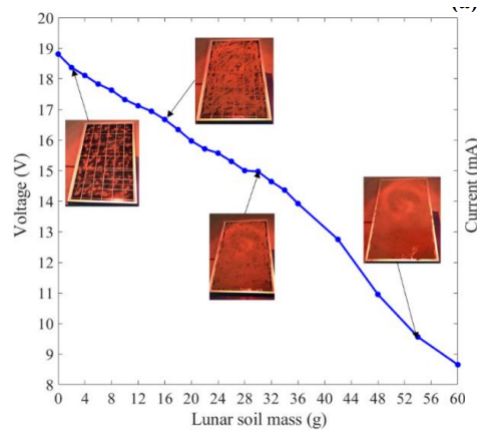


Figure A.2: voltage of the solar panels to dust mass[19]

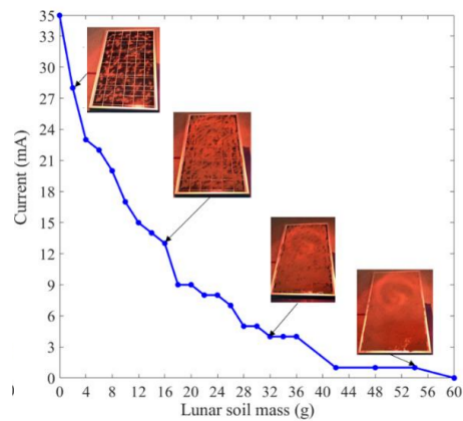


Figure A.3: Current of the solar panels to dust mass [19]

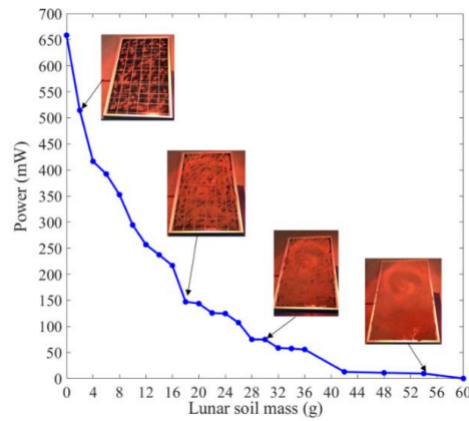


Figure A.4: Power of the solar panels to dust mass [19]

A.5. Electrostatics

The electric field can be expressed as contribution of multiple point charges [47]:

$$\mathbf{E}_1 = \frac{q_1 (\mathbf{R} - \mathbf{R}_1)}{4\pi\epsilon |\mathbf{R} - \mathbf{R}_1|^3} \quad (\text{V/m}) \quad (\text{A.4})$$

Electric field due to charge distribution inside a volume is expressed as[47]:

$$\mathbf{E} = \int_{v'} d\mathbf{E} = \frac{1}{4\pi\epsilon} \int_{v'} \hat{\mathbf{R}}' \frac{\rho_v dv'}{R'^2} \quad (\text{A.5})$$

A.5.1. Capacitance

Capacitance is described by the following equation[47]

$$C = \frac{Q}{V} \quad (\text{A.6})$$

The charge can be expressed with the Gauss law, where the integral of the surface is equal to the charge.

$$Q = \int_S \rho_s ds = \int_S \epsilon \hat{\mathbf{n}} \cdot \mathbf{E} ds = \int_S \epsilon \mathbf{E} \cdot d\mathbf{s} \quad (\text{A.7})$$

Using:

$$V = V_{12} = - \int_{P_2}^{P_1} \mathbf{E} \cdot d\mathbf{l} \quad (\text{A.8})$$

And equation A.6 gives rise to the following equation for capacitance:

$$C = \frac{\int_S \epsilon \mathbf{E} \cdot d\mathbf{s}}{- \int_l \mathbf{E} \cdot d\mathbf{l}} \quad (\text{A.9})$$

A.6. Transmission line

The propagation constant for a transmission line is defined as [47]:

$$\gamma = \sqrt{(R'j\omega L')(G' + j\omega C')} \quad (\text{A.10})$$

Because inductance and conductance are neglected for EDS. The propagation constant is defined as:

$$\gamma = \sqrt{R'j\omega C'} \quad (\text{A.11})$$

The voltage at any point in the EDS system can be determined by filling in the following equation.

$$V(z) = A \cdot e^{-\gamma \cdot z} \quad (\text{A.12})$$

We would like to know the behavior at the end of the electrode

$$V(\omega) = A \cdot e^{-\sqrt{R' j \omega C'} \cdot l} \quad (\text{A.13})$$

A.6.1. Electrode Resistance

The equation for wire resistance per meter is given by:

$$R' = \frac{1}{\sigma} \cdot \frac{1}{A} \quad (\text{A.14})$$

where R' is the resistance per unit length of the wire, ρ is the resistivity of the material that is the inverse of the conductivity given by $\rho = \frac{1}{\sigma}$, A is the cross-sectional area of the wire.

A.6.2. Series resistance

The resistance of a co planar conductor can be described with the following equation:

$$R_{dc} = \frac{2l}{\sigma_0 \sigma_r w h} \quad (\text{A.15})$$

where w is the width of the conductor and h is the height of the conductor.

A.6.3. Co planar Capacitance

Calculating the electric field is difficult of the system. This is why numerical calculations are done. And also a simplification is made by using parallel wires instead of volume charge distributions.

The electrostatics screen consist of parallel electrodes which are approximated as geometric squares. A simple equation of parallel wires can be used to estimate the capacitance. [57]

$$C' = \frac{\pi \epsilon}{\text{arcosh}\left(\frac{d}{2a}\right)} = \frac{\pi \epsilon}{\ln\left(\frac{d}{2a} + \sqrt{\frac{d^2}{4a^2} - 1}\right)} \quad (\text{A.16})$$

This equation is mainly valid when the distance is far greater than the width of the electrodes [48].

To have a better approximation of the capacitance R. Zypman[48] came up with another equation that describes the capacitance of a co-plainer electrode. But the simple equation A.16 is still handy for sanity checks.

The equation R. Zypman[48] proposed is given by:

$$C' = \frac{\pi \epsilon}{r} \frac{K\left(\frac{r^2-1}{r^2}\right)}{\frac{1}{r+1} \left[2(\gamma + \ln(4))K\left(\left(\frac{r-1}{r+1}\right)^2\right) - \pi \left[F_3\left(\frac{1}{2}, \frac{1}{2}, 1, \left(\frac{r-1}{r+1}\right)^2\right) + F_2\left(\frac{1}{2}, \frac{1}{2}, 1, \left(\frac{r-1}{r+1}\right)^2\right) \right] \right] + \ell n\left(\frac{r+1}{r-1}\right) \frac{1}{r} K\left(\frac{r^2-1}{r^2}\right)} \quad (\text{A.17})$$

where r is defined as:

$$r = \frac{p + 2 \cdot w}{p} \quad (\text{A.18})$$

and a is defined as $a = \frac{d-w}{2}$ and b is $\frac{d}{w}$, d is the separation distance and w is the width of the electrodes. K is the **Complete elliptic integral of the second kind** which is defined as

$$F(\phi, k) = \int_0^\phi \frac{d\theta}{\sqrt{1 - k^2 \sin^2 \theta}} \quad (\text{A.19})$$

This integral can be expressed as a power series. Which is defined as followed:

$$K(k) = \frac{\pi}{2} \sum_{n=0}^{\infty} \left(\frac{(2n)!}{2^{2n}(n!)^2} \right) \quad (\text{A.20})$$

F3 and F2 are **Gauss hypergeometric function** which is defined as

$$F(a, b, c, z) = \sum_{n=0}^{\infty} \frac{(a)_n (b)_n}{(c)_n} \frac{z^n}{n!}, \quad (\text{A.21})$$

The Co planar capacitance function A.17 uses the Gauss hypergeometric function with two derivatives, one with respect to the second term and one with respect to the third term. Because of the complexity and nature of the sum its difficult to do these derivatives analytically. Lucky these equations are available within SciPy [58] which is a python package. The derivative can be done numerically which is simply done by the following equation:

$$\frac{f(x+h) - f(x)}{h} \quad (\text{A.22})$$

This is a really simple derivative equation.

The dielectric constant of the surface material is generally higher, so that means that the capacitance may be bigger. Than initially thought.

An important result from the capacitance equation is that the capacitance primarily consists of the surface area of the electrode which is also inside the capacitance equation A.9. Therefore, the capacitance is not dependent on height of the electrodes.

A.7. Optics

A.7.1. transmittance

The transmittance is defined as the ratio between the incident and transiting electric field. It depends on the incident θ_i and the transmission angle θ_t This is defined by following equation[47].

$$T_{\perp} = \frac{P_{\perp}^t}{P_{\perp}^i} = \frac{|E_{\perp}^t|^2}{|E_{\perp}^i|^2} \frac{\eta_1}{\eta_2} \frac{A \cos \theta_t}{A \cos \theta_i} = |\tau_{\perp}|^2 \left(\frac{\eta_1 \cos \theta_1}{\eta_2 \cos \theta_1} \right), \quad (\text{A.23})$$

There τ is the **Transmission coefficient**. We will simplify this problem by assuming that the incident of the light is perpendicular to the surface this is when $\theta_i = \theta_t$

$$\tau = \frac{2\eta_2}{\eta_2 + \eta_1} \quad (\text{A.24})$$

The transmittance is given by the following equation [47]:

$$T = |\tau|^2 \left(\frac{\eta_1}{\eta_2} \right) \quad (\text{A.25})$$

η_1 and η_2 is the **intrinsic impedance** for the two mediums. For simplicity we will use the equation for

A.7.2. Complex refraction index

The refractive index is a measure of the bending of a ray of light when it passes from one medium to another.

The complex refraction index also accounts for absorption in a medium. This is defined as:

$$\underline{n} = n + i\kappa. \quad (\text{A.26})$$

where n is the refractive index and κ is the **optical extinction coefficient**

Kappa relates to the absorption coefficient with the following equation

$$\alpha = \frac{4\pi\kappa}{\lambda_0} \quad (\text{A.27})$$

Alpha also relates to the **Penetration depth** [47].

$$\delta_p = \frac{1}{\alpha} \quad (\text{A.28})$$

Case of uniform attenuation the **Transmittance** can be expressed as function of the length l and optical extinction coefficient κ defined by

$$T = e^{-\alpha \cdot h} \quad (\text{A.29})$$

where h is the thickness of the material

For indium tin oxide (ITO) the **Complex refraction index** is determined experimentally and accessible by the website of Polyanskiy [59]

A.7.3. Attenuation

$$\epsilon' = \epsilon \quad (\text{A.30})$$

$$\epsilon'' = \frac{\sigma}{\omega} \quad (\text{A.31})$$

Using the theory for plane wave propagation in a medium where the **attenuation constant** α and **phase constant** β are described by the following equation [47].

$$\alpha = \omega \left\{ \frac{\mu\epsilon'}{2} \left[\sqrt{1 + \left(\frac{\epsilon''}{\epsilon'} \right)^2} - 1 \right] \right\}^{1/2} \quad (\text{Np/m}), \quad (\text{A.32})$$

and beta β

$$\beta = \omega \left\{ \frac{\mu\epsilon'}{2} \left[\sqrt{1 + \left(\frac{\epsilon''}{\epsilon'} \right)^2} + 1 \right] \right\}^{1/2} \quad (\text{rad/m}). \quad (\text{A.33})$$

Because we are interested in the losses in transmission of an indium oxide conductor. We can use a simplification of the above equations. By the following equations [47].

$$\alpha \approx \omega \sqrt{\frac{\mu\epsilon''}{2}} = \omega \sqrt{\frac{\mu\sigma}{2\omega}} = \sqrt{\pi f \mu \sigma} \quad (\text{A.34})$$

And beta β is the same as alpha

$$\beta = \alpha \approx \sqrt{\pi f \mu \sigma} \quad (\text{rad/m}), \quad (\text{A.35})$$

The Intrinsic Impedance can be approximated as

$$\eta_c \approx \sqrt{j \frac{\mu}{\epsilon''}} = (1+j) \sqrt{\frac{\pi f \mu}{\sigma}} = (1+j) \frac{\alpha}{\sigma} \quad (\Omega). \quad (\text{A.36})$$

A.8. Solar panel

A.8.1. Short circuit current

The short circuit current through the solar cell is described as [9]

$$I_{sc} = -q \int_{\lambda_1}^{\lambda_2} EQE(\lambda) \Phi_{phy}^{AM1.5} d\lambda, \quad (A.37)$$

Where q is the elementary charge of a electron. EQE is the quantum efficiency and ϕ is the spectral photon flux.

Determine the current through each solar cell of a triple junction solar cell. The following three equations are used.

$$I_{sc-1} = -q \int_{300}^{600} EQE(\lambda) \Phi_{phy}^{AM0} d\lambda, \quad (A.38)$$

$$I_{sc-2} = -q \int_{600}^{900} EQE(\lambda) \Phi_{phy}^{AM0} d\lambda, \quad (A.39)$$

$$I_{sc-3} = -q \int_{900}^{1900} EQE(\lambda) \Phi_{phy}^{AM0} d\lambda, \quad (A.40)$$

These integrals are continuous integrals because the radiance ϕ is the delay in the experiment. Only numerical analysis can be used. That is why the short circuit current for all three integrals has to be done numerically. This numerical integral is defined by rewriting the equation A.37. This results in

$$I_{sc} = -q \sum_{\lambda=200nm}^{1700nm} EQE(\lambda) \Phi_{phy}^{AM1.5}(\lambda) d\lambda, \quad (A.41)$$

A.8.2. J-V Curve

The J-V characteristic of a solar panel can be described by the following equation.

$$J(V) = J_0 \left[\exp\left(\frac{qV}{k_B T}\right) - 1 \right] - J_{ph}. \quad (A.42)$$

where J_0 is the **Saturation current density**, q the charge, K_b is the Boltzmann constant, T is the temperature in kelvin and j_{ph} is the photon current.

A.8.3. Open circuit voltage

The open circuit voltage of each solar cell depends on the recombination of electron-hole pairs. This is described by equation A.43[9].

$$V_{oc} = \frac{k_B T}{q} \ln\left(\frac{J_{Ph}}{J_0} + 1\right) \approx \frac{k_B T}{q} \ln\left(\frac{J_{Ph}}{J_0}\right) \quad (A.43)$$

Due to the complexity of the recombination mechanisms and the difficulty of making an estimation for J_0 and the unknown construction of the solar panel. J_0 is assumed to be around $J_0 = 2e - 13$. This is taken from [60].

A.8.4. Solar panel Efficiency

The maximum efficiency of the solar panel is reached when the solar panel operates at the maximum power point.

A.8.5. Conductance of insulation medium

using the approximation of two wires.

$$G' = \frac{\pi \cdot \sigma}{\ln((D/d) + \sqrt{(D/d)^2 - 1})} \quad (\text{A.44})$$

A.9. Effects of transmission line

In [48] its stated that the effect of transmission lines may not be ignored if the following equation holds.

$$\frac{l}{\lambda} \geq 0.01 \quad (\text{A.45})$$

where l is the length of the transmission line and λ is the wave length.

lambda is given by the following equation

$$\lambda = \frac{u_p}{f} \quad (\text{A.46})$$

Substituting $u_p = \frac{c}{\sqrt{\epsilon_r}}$ results in[48]

$$\frac{\sqrt{\epsilon_r} \cdot l}{c \cdot f} \geq 0.01 \quad (\text{A.47})$$

where ϵ_r is the relative permittivity.

A.9.1. Characteristic impedance of the line

Characteristic impedance of a transmission line is defined as: [48]

$$Z_o = \sqrt{\frac{R' + j' \omega L}{G' + j \omega C'}} \quad (\Omega) \quad (\text{A.48})$$

A.9.2. Reflection

Reflection is a phenomina where a traveling wave will reflect back to the source.

$$T = |T|e^{j\theta_r} \quad (\text{A.49})$$

The reflection coefficient of a simple transmission line is defined as

$$T = \frac{Z_l - Z_0}{Z_l + Z_0} \quad (\text{A.50})$$

Open end problem. The transmission line is terminated with an open end. This causes a reflection of -1.

A.9.3. Phase shift

The electrode have a finite length because the amount of electrodes and the use of a PWM signal which contains high frequency components. There can be a phase delay on the plane of electrodes. Which manifest itself with the following relation:

$$\phi = \frac{\omega l}{c} \quad (\text{A.51})$$

Where c is the speed of light, l is the length of the electrode and ω the angular frequency of the signal.

A.10. Electric field strength needed at different solar panel angles

Due to the inclination ϕ the equation 5.9 has to be rewritten with an additional $\cos(\phi)$ term. where ϕ is the angle between the solar panel and the rover. $0 < \phi < \frac{\pi}{2}$

$$|E_y| \geq \sqrt{\frac{4}{3\epsilon_0} \pi r_d^2 p G_s \cdot \cos(\phi) + \frac{c \cdot s^2}{\pi \cdot r_d}} \quad (\text{A.52})$$

A.11. Code

Listing A.1: Python functions for construction of plots

```

import numpy as np
import sympy as smp
import matplotlib.pyplot as plt
import pandas as pd
import scipy as sc

# reduction of solar irradiance /m^2
def ques(res, lunardays=1):
    Q = 3.25
    N = 4000 * lunardays
    Ap = ((50e-6/2)**2) * np.pi
    r_d= (50e-6/2)
    g = (4000* (50e-6/2)**3 * (4/3) * 2750 * np.pi) * 1e3 * lunardays
    return res * np.exp(-2*N*Ap*Q), g

def setup_frame(w,p,h):
    #h = 0.1 # in um
    ath = 0.01
    data = [
        {
            'width□(mm)':w,
            'pitch□(mm)':p,
            'height□μ(m)':h,
            'Relative□Efficiency□η()': ITO_Effic(h),
            'Efield□Coverage': E_field_coverage(w,p,ey_escape(s=0.75,c=5.14e
                -2,r_d=10e-6),ath),
            'Switching□frequency': f_switch(w,p),
            'Area□Coverage': n(w,p),
            'End□of□transmission': respon(w,h,32e-2)
        }
    ]
    df = pd.DataFrame(data)
    print (df)
    return df

# Returns the relative efficiency of I
def ITO_Effic(l):
    return ITO_Power(l)/ITO_Power(0)

# Returns the efficiency of the solar panel with ITO of I
def ITO_Power(l):
    lam, spec, Tret = z1 = spectrum(l)

    I = J(lam, spec)
    V = np.sum(Voc(np.array(np.abs(I))))
    return np.max(I)*30e-4*V*0.83

# Estimate of the J-V curve

```

```

def iv_curve(v):
    T = 300
    k = 1.380649e-23
    q = 1.60217663e-19
    Jsc = 0.519/(30e-4)

    Jo=2e-13 # Gussed value from Chapter_IC-5_-

    J = Jo * np.exp((q*v)/(k*T)) - Jsc
    return J

def Voc(Jsc):
    T = 300
    k = 1.380649e-23
    q = 1.60217663e-19
    Jo=2e-13 # Gussed value from Chapter_IC-5_-
    return ((k*T)/q)*np.log(Jsc/Jo)

# Returns the current desnity of each solar panel
def J(lam, res):
    # lam, spec = AM0()
    lam, res = jsc(lam, res) # get current density
    lam = lam[:-1]
    # print(lam, res)

    # print(np.size(lam), np.size(res))
    # print(res[np.isclose(lam, 650,1)])

    # Find where the spectrum is close
    J1 = res[np.isclose(lam, 650,1e-1)][0]
    J2 = res[np.isclose(lam, 900,1e-1)][0] - J1
    J3 = res[np.isclose(lam, 1700,1e-1)][0] - (J1 + J2)

    if np.size(J1)==0 or np.size(J2)==0 or np.size(J3)==0:
        print("error□lenght")
    # else:
        # print(J1, J2, J3)

    return [J1, J2, J3]

# Plot the J-V curve
def pltiv():
    v = np.linspace(0,2,100)
    J = iv_curve(v)
    # plt.plot(v,J)
    # plt.ylim(-200,10)
    # plt.xlabel("Voltage (V)")
    # plt.ylabel(r"Current density $(A/m^2)$")

# returns the current density as function of wavelenght
def jsc(lam, p):
    # lam, p = AM0()

```

```

q = 1.60217663e-19
h = 6.62607015e-34
c = 299792458

def temp(p,lam):
    perc = [0.85, 0.9, 0.60] # EQE efficiency
    i = 0
    if (lam < 650):
        i = 0
    elif (650 < lam < 900):
        i = 1
    else:
        i = 2
        # eqe * phi
    return perc[i] * ((lam * p) / (h * c))

# make a array of eqe * phi
eqe_res = []
for i in range(0, len(lam)-1):
    eqe_res.append(temp(p[i], lam[i]))

s = [0]

# int(^)
# numerical integration:
for i in range(0, len(eqe_res)-1):
    s.append(s[i] + (( (eqe_res[i+1]+eqe_res[i])/2) * ((lam[i+1]-
        lam[i])*1e-9) ))

# plt.plot(lam[:-1], -q*np.array(s))
# plt.xlim(0,2500)
# plt.ylim(-0.2,0.1)
# plt.title("current density")
# plt.show()

# eqe_func = EQE(phi)
return lam, -q*np.array(s)

def power_loss(w,p):
    return n(w,p)*IOT_Power_loss()

# returns the minimum electric field at position h above the electrode
def E_bounds(w,p,h):
    x, field = Efield_at(w,p,h)
    return np.min(field), np.max(field)

# Returns the coverage as % which fullfills the dust removal condition
def E_field_coverage(w,p,Emin,ath=0.01):
    x,y = Efield_at(w,p,ath)
    return np.sum(y > Emin)/np.size(y)

# returns a array of field strenght above a electrode at high h

```

```

def Efield_at(w,p,h):
    p = p/1000
    w = w/1000
    h = h/1000
    ex, ey = e_field(w,p)
    x = np.linspace(0,p+2*w,100)
    Eamp = np.sqrt(ex(x,h)**2 + ey(x,h)**2)

    plt.plot(x*1000,Eamp)
    plt.show()

    return x, Eamp

# transmission line response of ITO plot
def respon(w,h,l ,sigma=1.3e4):
    w = w/1000
    h = h*1e-6

    # Todo: Capacitance per unit lenght:
    C= 120e-14/8.5e-2

    # Electrical resistance per unit lenght:
    A = w*h
    R = (1/sigma) * (1/A)
    return np.exp(-np.sqrt(R*1j*C)*l)

# Coverage factor
def n(w,p):
    w = w/1000
    p = p/1000
    return w/(w+p)

# trying to interpolate the AMO spectrum with IOT spectrum.
def spectrum(h=1): # h is 1um
    Amlam, Ampower = AMO()
    lotlam , lot = IOT(h)

    spec = []
    Tret = []
    i = 0
    for lam in Amlam:
        index = np.isclose(lotlam , lam,1e-02)
        T = lot[index]
        if np.size(T) > 0:
            spec.append(T[0] * Ampower[i])
            Tret.append(T[0])
        elif i > np.size(lotlam):
            # Extending the transmission (good aproximate)
            spec.append(lot[len(lot)-1] * Ampower[i])
            Tret.append(lot[len(lot)-1])
        else:
            spec.append(0)

```

```

        Tret.append(0)
        i = i + 1

# return lambda, specturm, and absorption
# show results visually
# plt.plot(Amlam[:1060], Ampower[:1060], label="AM0")
# plt.plot(Amlam,spec, label="spectrum after")
# plt.plot(Amlam,Tret, label="Absoprtion Coefficient")
# plt.legend()
# plt.xlim(0,Amlam[1060])
# plt.title("Spectrum alternation")
# plt.show()
return Amlam, np.array(spec), Tret

# power in w/m^-2
def AM0_power():
    lam, irradiance = AM0()

    power = [0]
    for i in range(0, len(lam)-1):
        power.append(power[i] + ((irradiance[i+1] + irradiance[i])/2)*(lam[i
            +1]-lam[i]))
    # plt.plot(lam[:1438],power[:1438])
    # plt.title("Power of spectrum")
    # plt.show()
    return lam, power # correct result after integration ~1.3kw

# AM0 spectrum
def AM0():
    # loading in AM0
    df = pd.read_excel(r'AM0.xls')
    lam = df['Wavelength[nm]']
    irradiance = df['W*m-2*nm-1']
    # plt.plot(lam[:1438],irradiance[:1438], label="AM0")
    # plt.title("AM0 Spectrum")
    # plt.xlabel("Wavelength (nm)")
    # plt.show()
    return np.array(lam), np.array(irradiance)

def IOT_Power_loss():
    lam, T = IOT()
    return np.sum(T) / np.size(T)

# Transmission model
# h = 1 # um
def IOT(h=1):
    data = np.loadtxt('knvalues.txt', skiprows=1)
    lam = data[:, 0] # the wave lenght is already defined by measurment.
    n = data[:, 1]
    k = data[:, 2]
    a = (4*np.pi*k)/lam #um^-1
    T = np.exp(-1*a*h)
    return lam*1e3, T # return the wave lenght in nm and T (tranmission
        coefficient) as ratio (0-1)

```

```

# Escape field needed
def ey_escape(s=0.9,c=5.14e-2,r_d=1e-6):
    E0_eval = 8.854e-12
    Ey = np.sqrt( (c*(s**2))/(np.pi * r_d*E0_eval))
    print("Escape field: " + np.format_float_scientific(Ey) + " for
          particle of size: " + str(r_d))
    return Ey

# Determens the switching frequency of the circuit
def f_switch(w,p,Ex=8e5,q=0.02e-3):
    w = w/1000
    p = p/1000
    f = 1/np.sqrt(((w+p)*2) / (q*np.abs(Ex)))
    return f

# Give a electric field magnitude at the middle of the electrodes
def evaluate(w,p,h_eval):
    w = w/1000
    p = p/1000
    h_eval = h_eval/1000

    ex, ey = e_field(w,p)
    return np.sqrt(ex((w+0.5*p),h_eval)**2 + ey((w+0.5*p),h_eval)**2)

# w and p are in mm
def vec_plot_fnc(w,p):
    w = w/1000
    p = p/1000

    x,y = np.meshgrid(np.linspace(-w*2,w*8,60),np.linspace(0.00001,p*5,60)
    )
    ex, ey = e_field(w,p)
    label = "Electrical Field w=0.13, p=0.3"
    vec_plot(x*1000,y*1000,ex(x,y),ey(x,y),label)
    plt.plot([0, w*1000], [0,0], color="red", linewidth=5) # plot the
    first electrode
    plt.plot([(w + p)*1000, (2*w + p)*1000], [0,0], color="red", linewidth
    =5) # plot the second electrode

def vec_plot(x,y,u,v,label):
    fig = plt.figure(figsize=(10, 5))
    plt.quiver(x,y,u,v, width=0.0015, scale_units='inches')
    plt.title(label)
    plt.xlabel('x(mm)')
    plt.ylabel('y(mm)')
    plt.xlim(np.min(x), np.max(x))
    plt.ylim(np.min(y), np.max(y))
    return fig

```

```

# fil = is the treshold where values are taken out
def vec_filter_y(x,y, fil):
    x[ np.abs(y) < fil ] = np.nan
    y[ np.abs(y) < fil ] = np.nan
    return x, y

def e_field(width_electrode, pitch_electrode):
    px, py, pz = smp.symbols('p_x□p_y□p_z', real=True) # axis are real
    values.
    x, y, e, Q, w, g = smp.symbols('x□y□ε□q□w□g')

    # Making a line charge
    pv = Q/(2*w)

    # constructing E Field
    E_int = smp.Matrix([1/(smp.sqrt(px**2 - 2*px*x + py**2 + x**2)), -(px-
        x)/(py*smp.sqrt((px-x)**2 + py**2))])
    E_int = E_int*pv*(1/(4*smp.pi*e))

    E_int_wg = (E_int.subs(x,w) - E_int.subs(x,0)) + (-E_int.subs(x,2*w+g)
        + E_int.subs(x,w+g))

    E0 = 8.8541878128e-12 # Permittivity of free space
    # width_electrode = 0.0003
    # pitch_electrode = 0.004
    # qdis = (5.48e-12) * 1000 *0.001# from comol simulation

    # Charge? using simple estimate
    d = width_electrode+ pitch_electrode
    a = width_electrode/2
    qdis = (np.pi*E0 / np.arccosh(d/(2*a))) * 3.5 * 0.5 * 0.7 # fitting
        parameter :c

    # Filling in:
    E_int_wg_final = E_int_wg.subs(e, E0).subs(Q, qdis).subs(w,
        width_electrode).subs(g, pitch_electrode)

    # Making Electric field :)
    Ex_f = smp.lambdify([px, py], E_int_wg_final[0], 'numpy')
    Ey_f = smp.lambdify([px, py], E_int_wg_final[1], 'numpy')

    return Ex_f, Ey_f

```

B

Implementing Electrodes

B.1. Prototype

The prototype electrodes that were constructed on FR-4. This is a designate from the National Electrical Manufacturers Association for glass-reinforced epoxy. This material consists of fiberglass and epoxy resin.

FR stands for flame retardant. Some properties are summarized in table below:

Table B.1: Electrical characteristics of FR-4 from [61]

3.9 – 4.7	Dielectric constant ϵ_r Dielectric strength Relative permittivity
20MV/m = 20kv/mm	
4.4	

B.1.1. Creating a spiral electrode

The spiral design is difficult and tedious to draw by hand. Therefore, the shape is parameterized and written in a software function for which PCB software tool KICAD [62] is used.

The basic mathematics consist of a circle equation with radius r_n where n is the phase number:

$$\begin{bmatrix} x \\ y \end{bmatrix} = \begin{bmatrix} r_n \cdot np \cdot \cos(\theta) \\ r_n \cdot np \cdot \sin(\theta) \end{bmatrix} \quad (\text{B.1})$$

r_n is initialized differently for each phase because no overlap is desired. r_n is written as a recursive formula as followed:

$$r_n[a + 1] = r_n[a] - r_{conv} \quad (\text{B.2})$$

Where a is a index value in domain \mathbb{Z} ,

This can be written non recursively in the form of

$$r_n[a] = r_{init} - a \cdot n \cdot r_{conv} \quad (\text{B.3})$$

Same applies for θ this is done recursively in code as

$$\theta[a + 1] = \theta[a] + \theta_{step} \quad (\text{B.4})$$

which can be written none recursively as

$$\theta = \theta_{init} + a \cdot \theta_{step} \quad (\text{B.5})$$

now by evaluating the following integral the lenght of the circle can be calculated:

$$\int_0^a (r_{init} - a \cdot r_{conv}) \cdot \quad (B.6)$$

By taking a final position of r_n we can calculate a by doing the following.

$$\frac{r_{init} - r_{final}}{r_{conv}} = a \quad (B.7)$$

by using the follow in formula the length of a spiral coil can be found as

$$L = \pi \cdot n \cdot \frac{(D + d)}{2} \quad (B.8)$$

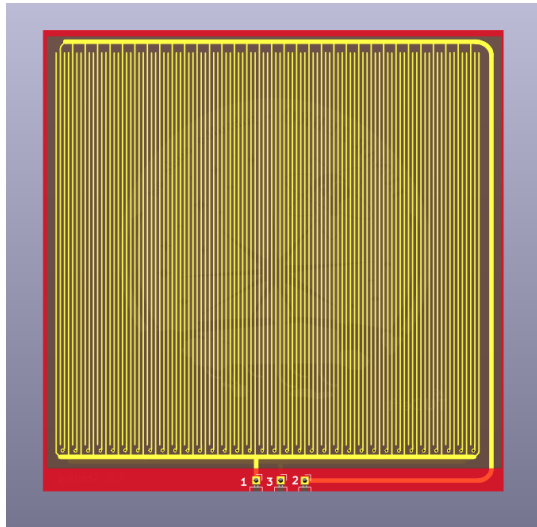
Where n is the number of rings, D is the outside diameter d is the inside diameter

The number of rings depend on the spacing and with of the electrodes. In general $n = \frac{D}{w_{electrode} + p_{electrode}}$
where w and p are the width and the pitch.

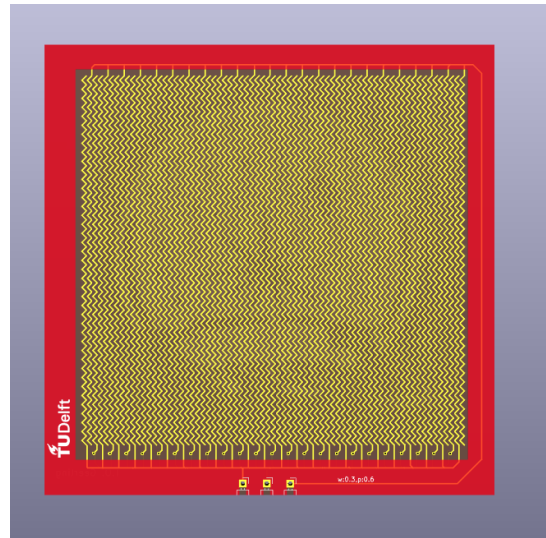
The code for generating these circles can be found in B.3

B.1.2. Images of design iteration 1

Below in Figures B.1a,, B.1c, B.1d, , the rendered images of the first iteration can be found.



(a) Parallel design 1



(b) Zigzag design 3



(c) Spiral design 4



(d) Spiral design 5

Figure B.1: Different constructed designs

B.2. Kicad automation scripts

In this section, the code is shown to generate the electrode patterns by automation. This is done with the python with the Kicad library "pcbnew".

Listing B.1: Code for generating zig-zag patterns

```
# "C:\Program Files\KiCad\6.0\bin\python.exe" "D:\Documents\KiCad\6.0\
  scripting\plugins\zigzag.py"
import pcbnew

pth = "electrodesv1\electrodesv1.kicad_pcb"
board = pcbnew.LoadBoard(pth)

# Nets for electrodes:
elec_nets = [pcbnew.NETINFO_ITEM(board, "elec1"), pcbnew.NETINFO_ITEM(
  board, "elec2"), pcbnew.NETINFO_ITEM(board, "elec3")]

print(elec_nets[0].GetNetCode())

for i in range(0, 3):
  board.Add(elec_nets[i])

def sump(pos1, pos2):
  return pcbnew.wxPoint(pos1.x + pos2.x, pos1.y + pos2.y)

def pos(x,y):
  return pcbnew.wxPoint(x * pcbnew.IU_PER_MM, y * pcbnew.IU_PER_MM)

# Addes a line to the pcb :)
def add_line(start, end, width, layer=pcbnew.F_Cu):
  segment = pcbnew.PCB_SHAPE(board) # PCB_SHAPE makes a line,
  PCB_TRACK makes a trace
  # segment.SetShape(pcbnew.SHAPE_T_SEGMENT)
  segment.SetStart(start)
  segment.SetEnd(end)
  segment.SetLayer(layer)
  segment.SetWidth(int(width * pcbnew.IU_PER_MM))
  board.Add(segment)

# Addes a track to the pcb :)
def add_track(start, end, width, elec_nummber, layer=pcbnew.F_Cu):
  segment = pcbnew.PCB_TRACK(board) # PCB_SHAPE makes a line,
  PCB_TRACK makes a trace
  # segment.SetShape(pcbnew.SHAPE_T_SEGMENT)
  segment.SetStart(start)
  segment.SetEnd(end)
  segment.SetLayer(layer)
  segment.SetWidth(int(width * pcbnew.IU_PER_MM))

  print(elec_nummber)

  segment.SetNetCode(elec_nets[elec_nummber].GetNetCode())
  board.Add(segment)
```

```

def outline_edge(pcbx, pcby):
    layer=pcbnew.Edge_Cuts
    add_line(pos(0,0), pos(0,pcbx), 0.1 , layer)
    add_line(pos(0,pcbx), pos(pcby,pcbx), 0.1, layer)
    add_line(pos(pcby,pcbx), pos(pcby,0), 0.1, layer)
    add_line(pos(pcby,0), pos(0,0), 0.1, layer)

# sp spacing between electordes in mm
# w width of electrodes in mm
# l length of electrodes in mm
# n number of electrodes
# of offset from the edge of the pcb so starting position

# def make_electrodes(sp, w, l, n, of):
#     elec_nummber = 0
#     for i in range(1, n):
#         add_track(pos( i * (sp+w), of), pos( i *(sp+w), l-2*of), w,
elec_nummber) # start (x,y), stop (x,y)
#         elec_nummber = elec_nummber + 1
#         if elec_nummber == 3:
#             elec_nummber = 0

# d = distance to zig zag
# l = length of zig zag
# L = total length of electrode
# Ne = electrode number
def make_zigzag(d,l,initpos, Ne): # makes on zizag increasing with 2L
    pos_vec = [pos(0,0), pos(-d,l), pos(0,2*l)]

    # superposition
    for i in range(0, pos_vec.__len__()):
        pos_vec[i] = sump(pos_vec[i], initpos)

    # Make the zig zag

    for ps in range(0, len(pos_vec)-1):
        add_track(pos_vec[ps], pos_vec[ps+1], 0.3, Ne)

    return pos_vec[2] # return end locationof electrode

# L = lengthe of electrode
# W = width of electrode
# d = distance to zig zag
# l = length of zig zag
# s = spacing between electrodes

def make_zigzag_mesh(L=100,W=100, d=1, l=1, s=2):
    initpos = pos(20,0)
    looppos = initpos
    ne = 0

```

```

    for z in range(0, round(W/(s+2*0.3))): # number of electrodes next to
        each other
        for i in range(0, round(L/(2*l))): # electrode lenght
            initpos = make_zigzag(d, l, initpos, ne)
            ne = ne + 1
            if ne == 3:
                ne = 0
            looppos = sump(looppos, pos(s+2*0.3,0)) #spacing between
                electrodes
            initpos = looppos

# main code:

# pcb outline:
pcb_lx = 100 # length of pcb in mm
pcb_ly = 100 # width of pcb in mm

# Going to define the electrodes here
sp = 0.6 # spacing between electordes in mm
w = 0.3 # width of electrodes in mm
l = 100 # length of electrodes in mm
of = 5 # offset from the edge of the pcb so starting position

# Calculate the number of electrodes
n_ele = round(100/(sp + w)) # number of electrodes
print("Number of electrodes: " + str(n_ele))

# doing stuff with pcb here:
make_zigzag_mesh(100, 100, 1, 1, sp)
outline_edge(pcb_lx, pcb_ly) # make the edge cut of pcb

pth_saved = "electrodesv1\sketch.kicad_pcb"
board.Save(pth_saved)

```

Listing B.2: Code for generating straight electrodes

```

# "C:\Program Files\KiCad\6.0\bin\python.exe" "D:\Documents\KiCad\6.0\
    scripting\plugins\continous.py"
import pcbnew

pth = "electrodesv1\electrodesv1.kicad_pcb"
board = pcbnew.LoadBoard(pth)

# Nets for electrodes:
elec_nets = [pcbnew.NETINFO_ITEM(board, "elec1"), pcbnew.NETINFO_ITEM(
    board, "elec2"), pcbnew.NETINFO_ITEM(board, "elec3")]

print(elec_nets[0].GetNetCode())

for i in range(0, 3):

```

```

board.Add(elec_nets[i])

def pos(x,y):
    return pcbnew.wxPoint(x * pcbnew.IU_PER_MM, y * pcbnew.IU_PER_MM)

# Addes a line to the pcb :)
def add_line(start, end, width, layer=pcbnew.F_Cu):
    segment = pcbnew.PCB_SHAPE(board) # PCB_SHAPE makes a line ,
    PCB_TRACK makes a trace
    # segment.SetShape(pcbnew.SHAPE_T_SEGMENT)
    segment.SetStart(start)
    segment.SetEnd(end)
    segment.SetLayer(layer)
    segment.SetWidth(int(width * pcbnew.IU_PER_MM))
    board.Add(segment)

# Addes a track to the pcb :)
def add_track(start, end, width, elec_nummber, layer=pcbnew.F_Cu):
    segment = pcbnew.PCB_TRACK(board) # PCB_SHAPE makes a line ,
    PCB_TRACK makes a trace
    # segment.SetShape(pcbnew.SHAPE_T_SEGMENT)
    segment.SetStart(start)
    segment.SetEnd(end)
    segment.SetLayer(layer)
    segment.SetWidth(int(width * pcbnew.IU_PER_MM))

    print(elec_nummber)

    segment.SetNetCode(elec_nets[elec_nummber].GetNetCode())
    board.Add(segment)

def outline_edge(pcbx, pcby):
    layer=pcbnew.Edge_Cuts
    add_line(pos(0,0), pos(0,pcbx), 0.1, layer)
    add_line(pos(0,pcbx), pos(pcby,pcbx), 0.1, layer)
    add_line(pos(pcby,pcbx), pos(pcby,0), 0.1, layer)
    add_line(pos(pcby,0), pos(0,0), 0.1, layer)

# sp spacing between electordes in mm
# w width of electrodes in mm
# l length of electrodes in mm
# n number of electrodes
# of offset from the edge of the pcb so starting position

def make_electrodes(sp, w, l, n, of):
    elec_nummber = 0
    flag_switch = 0

    layer_index = [pcbnew.User_1, pcbnew.User_2, pcbnew.User_3]
    for i in range(1, n):

```

```

# add_track(pos( i * (sp+w), of), pos( i *(sp+w), l-2*of), w,
    elec_nummber) # start (x,y), stop (x,y)
lay = layer_index[elec_nummber]

add_line(pos( i * (sp+w), of), pos( i *(sp+w), l-2*of), w, lay)

if flag_switch == 0:
    elec_nummber = elec_nummber + 1
else:
    elec_nummber = elec_nummber - 1
# make this pattern # 1 -> 2 -> 3 -> 2 -> 1
if elec_nummber == 2:
    flag_switch = 1
if elec_nummber == 0:
    flag_switch = 0

# main code:

# pcb outline:
pcb_lx = 100 # length of pcb in mm
pcb_ly = 100 # width of pcb in mm

# Going to define the electrodes here
sp = 0.6 # spacing between electordes in mm
w = 0.3 # width of electrodes in mm
l = 100 # length of electrodes in mm
of = 5 # offset from the edge of the pcb so starting position

# Calculate the number of electrodes
n_ele = round(100/(sp + w)) # number of electrodes
print("Number of electrodes: " + str(n_ele))
print("Total lenght of electrodes: " + str(n_ele * l-2*of))

# doing stuff with pcb here:
make_electrodes(sp, w, l, n_ele, of) # creating the electrodes
outline_edge(pcb_lx, pcb_ly) # make the edge cut of pcb

pth_saved = "electrodesv1\sketch.kicad_pcb"
board.Save(pth_saved)

```

Listing B.3: code for generating spiral electrodes

```

# "C:\Program Files\KiCad\6.0\bin\python.exe" "D:\Documents\KiCad\6.0\
    scripting\plugins\spiral.py"
import pcbnew
import numpy as np
pth = "electrodesv1\electrodesv1.kicad_pcb"
board = pcbnew.LoadBoard(pth)

```

```

# Nets for electrodes:
elec_nets = [pcbnew.NETINFO_ITEM(board, "elec1"), pcbnew.NETINFO_ITEM(
    board, "elec2"), pcbnew.NETINFO_ITEM(board, "elec3")]

print(elec_nets[0].GetNetCode())

for i in range(0, 3):
    board.Add(elec_nets[i])

def sump(pos1, pos2):
    return pcbnew.wxPoint(pos1.x + pos2.x, pos1.y + pos2.y)

def pos(x,y):
    return pcbnew.wxPoint(x * pcbnew.IU_PER_MM, y * pcbnew.IU_PER_MM)

# Addes a line to the pcb :)
def add_line(start, end, width, layer=pcbnew.F_Cu):
    segment = pcbnew.PCB_SHAPE(board) # PCB_SHAPE makes a line ,
    PCB_TRACK makes a trace
    # segment.SetShape(pcbnew.SHAPE_T_SEGMENT)
    segment.SetStart(start)
    segment.SetEnd(end)
    segment.SetLayer(layer)
    segment.SetWidth(int(width * pcbnew.IU_PER_MM))
    board.Add(segment)

# Addes a track to the pcb :)
def add_track(start, end, width, elec_nummber, layer=pcbnew.F_Cu):
    segment = pcbnew.PCB_TRACK(board) # PCB_SHAPE makes a line ,
    PCB_TRACK makes a trace
    # segment.SetShape(pcbnew.SHAPE_T_SEGMENT)
    segment.SetStart(start)
    segment.SetEnd(end)
    segment.SetLayer(layer)
    segment.SetWidth(int(width * pcbnew.IU_PER_MM))

    print(elec_nummber)

    segment.SetNetCode(elec_nets[elec_nummber].GetNetCode())
    board.Add(segment)

def add_arc(start, end, width, elec_nummber=1, layer=pcbnew.F_Cu):
    arc = pcbnew.PCB_ARC(board)
    arc.SetStart(start)
    arc.SetEnd(end)
    board.Add(arc)

def outline_edge(pcbx, pcby):
    layer=pcbnew.Edge_Cuts
    add_line(pos(0,0), pos(0,pcbx), 0.1, layer)
    add_line(pos(0,pcbx), pos(pcby,pcbx), 0.1, layer)

```

```

add_line(pos(pcbx,pcby), pos(pcbx,0), 0.1, layer)
add_line(pos(pcbx,0), pos(0,0), 0.1, layer)

# d = distance to zig zag
# l = length of zig zag
# L = total length of electrode
# Ne = electrode number
def make_zigzag(d,l,initpos, Ne): # makes on zigzag increasing with 2L
    pos_vec = [pos(0,0), pos(-d,l), pos(0,2*l)]

    # superposition
    for i in range(0, pos_vec.__len__()):
        pos_vec[i] = sump(pos_vec[i], initpos)

    # Make the zig zag

    for ps in range(0, len(pos_vec)-1):
        add_track(pos_vec[ps], pos_vec[ps+1], 0.3, Ne)

    return pos_vec[2] # return end location of electrode

# L = length of electrode
# W = width of electrode
# d = distance to zig zag
# l = length of zig zag
# s = spacing between electrodes

def make_zigzag_mesh(L=100,W=100, d=1, l=1, s=2):
    initpos = pos(20,0)
    looppos = initpos
    ne = 0
    for z in range(0, round(W/(s+0.3))): # number of electrodes next to
        each other
        for i in range(0, round(L/(2*l))): # electrode length
            initpos = make_zigzag(d, l, initpos, ne)
            ne = ne + 1
            if ne == 3:
                ne = 0
            looppos = sump(looppos, pos(s,0))
            initpos = looppos

def coil():
    spacing_coils = 0.13 + 0.3

    widthe = 0.13

    nmofounds = 100/2.4 # radius of the coil

    loop_angl = 0
    loops = 30000 * 4
    stepsize = 0.05

```

```

n_iterations_circle = round(np.pi * 2 / stepsize)
radius_converg = spacing_coils / n_iterations_circle

y1 = []
x1 = []
r1 = nmofounds

r2 = nmofounds + spacing_coils
y2 = []
x2 = []

r3 = nmofounds + 2*spacing_coils
y3 = []
x3 = []
for i in range(0,loops):

    if r1 > 0:
        # Coil 1
        r1 = r1 - 3* radius_converg
        y1.append(r1 * np.sin(loop_angl))
        x1.append(r1 * np.cos(loop_angl))

    if r2 > 0:
        # coil 2
        r2 = r2 - 3* radius_converg
        y2.append(r2 * np.sin(loop_angl))
        x2.append(r2 * np.cos(loop_angl))

    if r3 > 0:
        # coil 3
        r3 = r3 - 3*radius_converg
        y3.append(r3 * np.sin(loop_angl))
        x3.append(r3 * np.cos(loop_angl))

    loop_angl = (loop_angl + stepsize)
    if r1 < 0 and r2 < 0 and r3 < 0:
        break

for i in range(0, len(x1)-1):
    add_track(pos(x1[i],y1[i]),pos(x1[i+1],y1[i+1]), widthe , 0)

for i in range(0, len(x2)-1):
    add_track(pos(x2[i],y2[i]),pos(x2[i+1],y2[i+1]), widthe , 1)

for i in range(0, len(x3)-1):
    add_track(pos(x3[i],y3[i]),pos(x3[i+1],y3[i+1]), widthe , 2)

# main code:

# pcb outline:
pcb_lx = 100 # length of pcb in mm
pcb_ly = 100 # width of pcb in mm

```

```
# Going to define the electrodes here
sp = 1.5 # spacing between electordes in mm
w = 0.13 # width of electrodes in mm
l = 100 # length of electrodes in mm
of = 5 # offset from the edge of the pcb so starting position

# Calculate the number of electrodes
n_ele = round(100/(sp + w)) # number of electrodes
print("Number of electrodes: " + str(n_ele))

# add_arc(pos(0,0), pos(10,10), pcbnew.F_Cu)
coil()
# doing stuff with pcb here:
# make_zigzag_mesh(100, 100, 1, 1, sp)

outline_edge(pcb_lx, pcb_ly) # make the edge cut of pcb

pth_saved = "electrodesv1\sketch.kicad_pcb"
board.Save(pth_saved)
```

C

Appendix C

C.1. Step-by-step plan testing iteration 1

The following operations have been performed on each design.

1. Turn on power supply
2. Turn on high voltage circuit fixed output
3. Measure DC voltage.
4. Measure capacitance by shorting 2 phases and measuring between those and the other phase
5. Measure 0.5g of dust, store in separate container
6. Turn on high voltage circuit with three phase pulse
7. Disperse the dust onto the electrode with funnel in the middle of the designed electrode uniformly over a period of 3 min
8. Turn off power supply
9. Remove dust from edges of PCB, and place whatever is left on the PCB on a scale
10. Measure the weight to determine the amount of dust remaining

C.2. Results Iteration 1

Table C.1: Measured and calculated capacitance of designs iteration 1

Design Number	Electrode pattern	Calculated Capacitance	Mutual capacitance
1	Straight electrodes	144pF	140pF
2	Straight electrodes	117pF	100pF
3	Zigzag electrodes	95pF	135pF
4	Spiral electrodes	120pF	140pF
5	Spiral electrodes	180pF	250pF



Figure C.1: Lab setup

C.3. Results Iteration 2

Table C.2: Measured and calculated capacitance of designs iteration 2

Design Number	Electrode pattern	Calculated Capacitance	Mutual capacitance
1	90 degree zigzag	220pF	300 pF
2	90 degree zigzag	130pF	180pF
3	90 degree zigzag	84pF	110pF
4	130 degree zigzag	140pF	230pF
5	130 degree zigzag	95pF	150pF
6	130 degree zigzag	55pF	77pF

C.4. Simulation Geometry Iteration 1

Both simulations are performed with a potential difference of 1kV between electrodes using the Electrostatics physics for an extremely fine mesh.

C.5. Indium tin oxide, ITO ($\text{In}_2\text{O}_3\text{-SnO}_2$) dataset

Refractive index and Extinction coefficient

Table C.3: Electrical Conductivity of Indium Tin Oxide (ITO)

Item	Value
Electrical Conductivity	$1.3 \times 10^4 \text{ S mm}^{-1}$

C.6. Solar panel Quantum efficiency

The Quantum Efficiency of the solar panel has been guessed, this is shown in table C.4. The guess is based on figure 3.3.

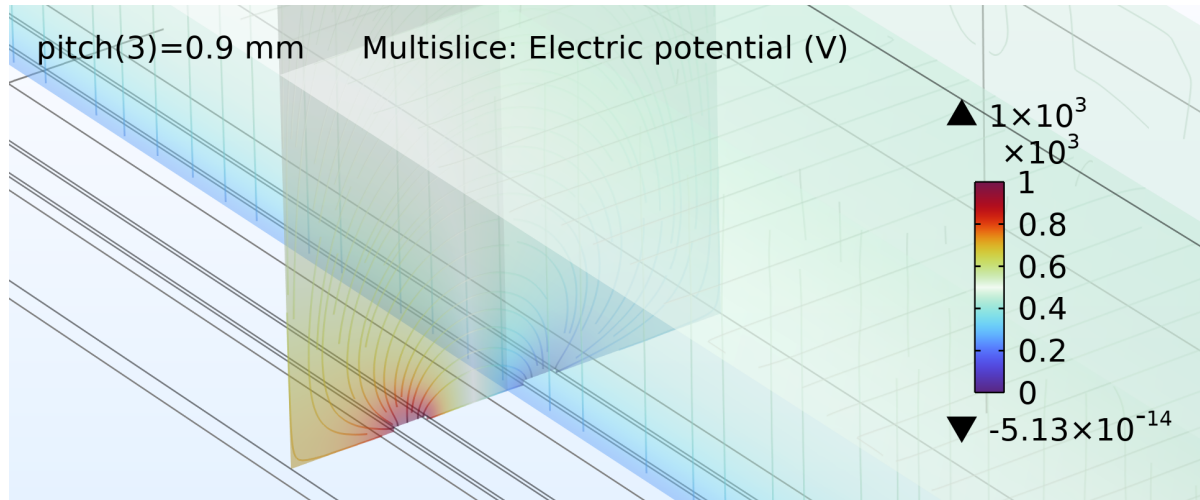


Figure C.2: Geometry and used sideview slice of parallel COMSOL simulation

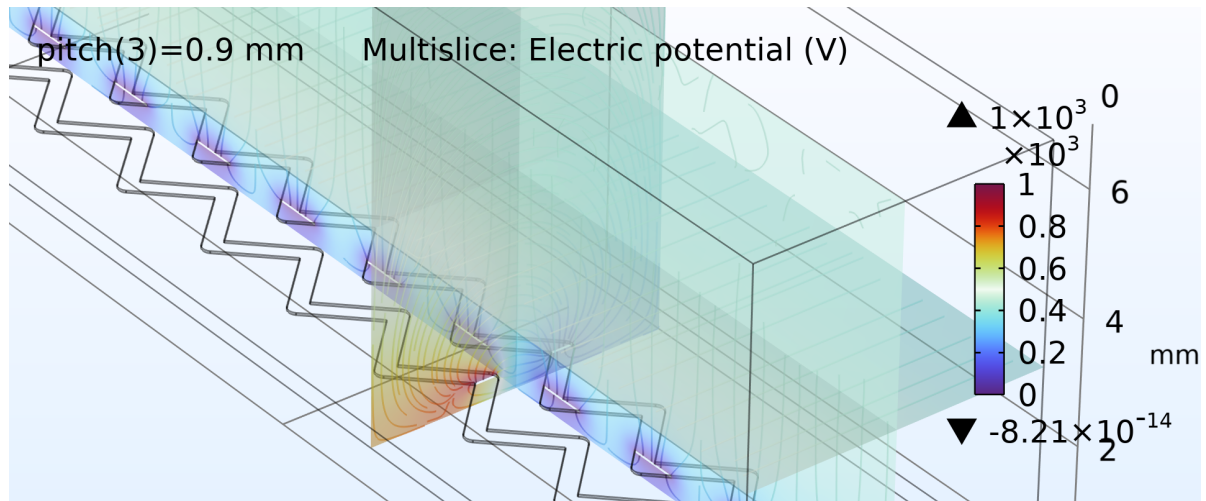


Figure C.3: Geometry and used sideview slice of zigzag COMSOL simulation

Table C.4: Educated guess of quantum efficiency

Wavelength Range	EQE Percentage
300-600 nm	87%
600-900 nm	90%
900-1600 nm	65%

C.7. Output Power Restoration (OPR) and Transmission Efficiency (TE)

When EDS is activated, the local electric field surrounding the fine electrodes becomes high and generates a space charge in the dielectric film [8-11]. The frequency of the applied voltage is in the range 1 to 20Hz. As the polarity of the electric field alternates, electrostatic charges are injected to the dielectric media from the electrodes or injected to the electrodes from the film. These space charge distributions surrounding the electrodes alter the applied electric field. The traveling wave causes the movement of charge depending upon the mobility of the charge in the medium. The charge injection and their motion play an important role in charging the dust particles deposited over the dielectric film surface. If the electric field is too high, the charge accumulation alter the electric field more significantly and cause aging of the medium or lead to a dielectric breakdown.



Figure C.4: Experimental observation finer dust stays on the electrodes than larger particles

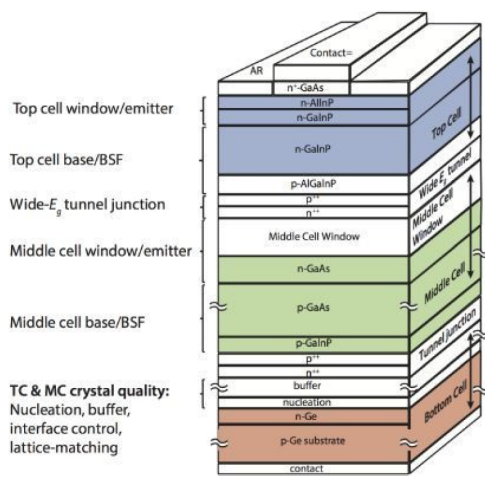


Figure C.5: Solar panel stack-up from [9]

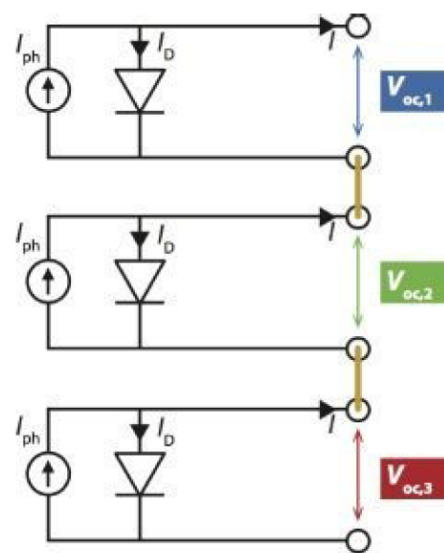


Figure C.6: Triple cell adapted from [9]